

On a Calderón preconditioner for the symmetric formulation of the electroencephalography forward problem without barycentric refinements

Viviana Giunzioni^a, John E. Ortiz G.^b, Adrien Merlini^c, Simon B. Adrian^d, Francesco P. Andriulli^{a,*}

^aDepartment of Electronics and Telecommunications, Politecnico di Torino, 10129 Turin, Italy

^bElectronic Engineering Department, Universidad de Nariño, Pasto 520002, Colombia

^cMicrowaves Department, IMT Atlantique, 29238 Brest, France

^dFakultät für Informatik und Elektrotechnik, Universität Rostock, 18051 Rostock, Germany

ARTICLE INFO

Article history:

Received 1 May 2013

Received in final form 10 May 2013

Accepted 13 May 2013

Available online 15 May 2013

Communicated by S. Sarkar

Keywords: Electroencephalography, EEG forward problem, Integral equations, Boundary element method, Calderón preconditioning, Preconditioner

ABSTRACT

We present a Calderón preconditioning scheme for the symmetric formulation of the forward electroencephalographic (EEG) problem that cures both the dense-discretization and the high-contrast breakdown. Unlike existing Calderón schemes presented for the EEG problem, it is refinement-free, that is, the electrostatic integral operators are not discretized with basis functions defined on the barycentrically-refined dual mesh. In fact, in the preconditioner, we reuse the original system matrix thus reducing computational burden. Moreover, the proposed formulation gives rise to a symmetric, positive-definite system of linear equations, which allows the application of the conjugate gradient method, an iterative method that exhibits a smaller computational cost compared to other Krylov subspace methods applicable to non-symmetric problems. Numerical results corroborate the theoretical analysis and attest of the efficacy of the proposed preconditioning technique on both canonical and realistic scenarios.

© 2022 Elsevier Inc. All rights reserved.

1. Introduction

Brain imaging techniques aim at fully determining the inner neural activity in terms of location, orientation, and intensity of the primary current, starting from some direct or indirect measurements of its correlated effects [49, 9]. Among them, source localization algorithms based on electroencephalographic (EEG) data are widely appreciated because of their high temporal resolution [37, 38] and of their compatibility with other imaging strategies, such as magnetoencephalography (MEG) [53], magnetic resonance imaging (MRI) [11, 32], and positron emission tomography (PET) [54]. This technology aims at reconstructing the equivalent volume brain sources from the measurement of the resulting potential distribution at the scalp [33, 46], which is known as the inverse EEG problem. Another inverse

*Corresponding author: .

e-mail: francesco.andriulli@polito.it (Francesco P. Andriulli)

problem relying on EEG modelling is the one of inferring the electrical parameters of the biological tissues, that is, the electrical conductivity and the permittivity, from surfacic electroencephalographic measurements, known as electrical impedance tomography (EIT) [14].

These problems are usually addressed through multiple iterative solutions of the forward EEG problem [26, 19, 23], which is the evaluation of the voltage function at the scalp resulting from a known electric activity inside the head [27, 28]. It follows, on the one hand, that the accuracy achievable in the resolution of the inverse problem is strictly limited by the one of the forward EEG problem; on the other hand, the resolution time is also affected by the complexity of the numerical model describing the forward problem [4]. These considerations evidence the crucial importance of determining realistic source and head models and defining affordable and efficient numerical schemes for the approximation of the electrostatic potential.

As far as the source modelling is concerned, equivalent currents, formed by the superposition of the effects of a number of infinitesimal dipoles, are widely considered to be an adequate representation of the electric brain activity whose effects are observed from the scalp [21], so that the majority of available numerical schemes relies on this approximation [19]. Many disparate head models have instead been developed and are still under active investigation [19]. They can be subdivided in two main categories. The methods of one of the categories assume that the electrical properties of the biological tissues constituting the head vary continuously so that a discretization of the full head volume is needed to numerically solve the problem; the formulations adopted in this case are both differential, traceable to the class of finite element method [7] or finite difference methods [13], and integral [48, 29] in nature, and can easily handle heterogeneities and anisotropies of the head tissues conductivity profiles. Alternatively, the methods of the other category assume piecewise-homogeneity, which allows subdividing the overall head into N compartments, representing separate biological tissues with distinct characteristics, such as, for example, the skin, the skull, the grey matter, and the white matter, and to approximate the above mentioned electrical properties as constant in each compartment [19]. By following this approach, there is no need for discretizing the full volumetric domain. Instead, a boundary element method (BEM) for the discretization of the integral formulation applied on the boundaries of the compartments only can be employed [35], allowing the reduction of the dimensionality of the problem by one. Moreover, boundary integral formulations applied to piecewise homogeneous head models can also handle anisotropies, as shown in [45]. The spherical head model (Figure 3b), that is, the representation of the head as the union of constant conductivity nested layers with spherical boundaries, for which the analytic solution of the forward problem is available [20, 65], and the realistic head model (Figure 3c), where the compartments in which the physical parameters are assumed constant are of general shape, are two examples of head models falling into this last category.

An historical overview of the most commonly employed boundary element schemes employed to solve the forward EEG problem is available in [35]. The single- and double-layer approaches summarized there are based on a partial exploitation of the representation theorem [39, 59]; the symmetric formulation instead, presented in [35], follows from a clever full use of the representation theorem and represents nowadays one of the most favorable choices for the numerical solution of the forward problem [19, 63]. The symmetric formulation has been shown to provide a higher level of accuracy in its results when compared to the single- and double-layer approaches, especially for shallow sources approaching the boundaries of the compartments [35, 63], which in turns leads to a higher reliability of the source localization algorithms based on it. This improvement comes at the cost of an higher computational complexity, that is, the linear system to be solved is approximately double in size with respect to the ones obtained from the single- and double-layer formulations. The increased cost is partially mitigated since the resulting interaction matrix becomes increasingly sparse when the number of compartments of the head model employed increases. Differently from the single- and double-layer formulations, which are second-kind integral equations, the symmetric formulation is of the first kind. As a consequence, its discretization results in a linear system whose conditioning worsens when the number of unknowns increases; this causes an increase of the solution time, a degradation of the solution accuracy, and, in some cases, prevents convergence altogether. This limitation actually prevents the application of the unpreconditioned symmetric formulation on complex realistic structures and opens the way of research toward efficient and effective preconditioning strategies, resulting in boundary integral formulations for the solution of the EEG forward problem that provide the same accuracy as the symmetric formulation and are immune to numerical instabilities.

In the last years, preconditioning strategies based on the Calderón identities have gained in popularity in the computational electromagnetics community [5]. They yield spectral equivalents of the inverse of the integral operators considered that are capable of preconditioning the formulation with respect to most sources of ill-conditioning, for example, denser discretization or lower frequencies. Calderón preconditioning has been successfully applied to full-

wave vectorial electromagnetic problems, such as the scattering from metallic [6, 8] and penetrable objects [10], as well as to scalar, acoustic problems [62, 60]. A Calderón preconditioning strategy for the EEG symmetric formulation has also been proposed in [42]. The Calderón preconditioning approach yields well-conditioned formulations in all these cases, at the cost of building a dual form of the BEM interaction matrix. Most of these schemes require the evaluation of dense electromagnetic operators on dual basis functions defined on the dual mesh, constructed for example via a barycentric refinement of the primal mesh, which leads to a non-negligible computational burden. Recently, a refinement-free Calderón preconditioning strategy for the electric field integral equation (EFIE) has been proposed [2], which leverages suitably modified graph Laplacians.

In this work, we propose a Calderón-like preconditioning for the symmetric formulation without resorting to integral operators discretized on the dual mesh, thereby reducing the computational cost compared with standard Calderón schemes such as [42]. The proposed formulation gives rise to a well-conditioned, symmetric, positive definite system of linear equations, amenable to fast iterative solvers, which remains stable under the different sources of ill-conditioning affecting the solution time of the non-preconditioned formulation. We obtain this by leveraging the Laplace-Beltrami operator in our preconditioning scheme, which can cheaply be discretized on the primal and on the dual mesh, and suitably applying it to our multiplicative preconditioning scheme. In contrast to [2], special care needs to be taken in our theoretical framework given that the underlying operator of the symmetric formulation is block-structured and that the final formulation is required not only to be immune to the dense-discretization, but also to the high-contrast breakdown [42]. Moreover, a consistent deflation strategy is introduced to avoid the nullspace of the symmetric formulation and the Laplace-Beltrami operator. Numerical results demonstrate the effectiveness of our scheme, both for canonical and realistic head models. Preliminary results, devoid of the theoretical apparatus presented here, have been presented in the conference contribution [24].

This paper is organized as follows: in Section 2 we review the forward EEG problem and the symmetric formulation for its numerical solution, providing the background and notation necessary for the following developments. Section 3 focuses on the numerical analysis of the two main sources of ill-conditioning plaguing the symmetric formulation. The novel preconditioning strategy is presented in Section 4 following a step-by-step process: after the introduction of a proof-of-concept preconditioning example, we first propose a deflation strategy to obtain a non-singular symmetric formulation, before finally outlining the proposed well-posed, well-conditioned formulation, whose favorable stability properties are proved in Section 4.4. Finally, Section 5 complements the theoretical analysis with a numerical study of the formulations under test, to illustrate the effectiveness of the preconditioning. This analysis is applied to both canonical spherical models, for which a comparison with analytic solutions is possible, and realistic models generated from magnetic resonance imaging (MRI) data. Moreover, source localization algorithms relying on the proposed formulation have been applied on the realistic head model, validating the use of this technology for neuroimaging purposes in biomedical applications.

2. Background and notation

In this section, we review the symmetric formulation for the solution of the forward EEG problem and set the notation for the elements needed to introduce the proposed formulation.

2.1. The forward EEG problem

The neural activity (i.e., the simultaneous activation of neurons situated in a region of the cortex) can be modeled by a primary current distribution, usually approximated as a combination of point dipoles [21]. The forward EEG problem consists in determining the potential induced by this current at the scalp.

Mathematically, the problem is described by Poisson's equation, which is obtained from the Maxwell's system in its quasi-static approximation [51]. This approximation is justified by the low frequency of the neural signals (mainly in the order of 1 Hz to 100 Hz [19]). Poisson's equation

$$\nabla \cdot (\sigma \nabla V) = \nabla \cdot \mathbf{j} \quad (1)$$

describes the relation between the dipolar current inside the brain \mathbf{j} (i.e., the source term of the problem) and the resulting potential distribution, V . In the forward problem, we are interested in solving the problem for spatial points $\mathbf{r} \in \Gamma := \partial\Omega$, where $\Omega \subset \mathbb{R}^3$ is an open set modeling the head, and the conductivity distribution $\sigma(\mathbf{r})$ of the biological

tissues is considered known. Since the conductivity outside the head is zero, no current flows out of the head leading to the Neumann boundary condition

$$\sigma \partial_{\mathbf{n}} V = 0 \quad \text{for } \mathbf{r} \in \Gamma, \quad (2)$$

where \mathbf{n} is the outward unit normal vector field characterizing the boundary Γ of the head domain.

2.2. The symmetric formulation

The symmetric formulation, which can be numerically solved in the BEM framework, relies on the piecewise-homogeneity assumption mentioned above, that is, we model the head as a set of non-overlapping, homogeneous compartments, representing distinct biological tissues. Mathematically, we describe this by introducing a set of N nested, open subsets of Ω , denoted as $\{\Omega_i\}_{i=1}^N$, with smooth boundaries, such that $\cup_{i=1}^N \bar{\Omega}_i = \bar{\Omega}$ and $\Omega_i \cap \Omega_{j \neq i} = \emptyset$. Furthermore, Γ_i denotes the boundary defined by $\Gamma_i := \bar{\Omega}_i \cap \bar{\Omega}_{i+1}$, on which \mathbf{n}_i is the unit-length normal vector directed towards Ω_{i+1} , and Ω_{N+1} is the exterior of Ω , that is, $\Omega_{N+1} := \mathbb{R}^3 \setminus \bar{\Omega}$. The notation employed is represented in Figure 3a. In this work, we will assume isotropic conductivity modelled by the piecewise constant function

$$\sigma(\mathbf{r}) = \sum_{i=1}^{N+1} \sigma_i I_{\Omega_i}(\mathbf{r}), \quad (3)$$

where σ_i is scalar and $I_{\Omega_i}(\mathbf{r})$ is the indicator function of Ω_i

$$I_{\Omega_i}(\mathbf{r}) := \begin{cases} 1 & \text{if } \mathbf{r} \in \Omega_i, \\ 0 & \text{otherwise.} \end{cases} \quad (4)$$

Under these conditions, the forward EEG problem can be rewritten as

$$\sigma_i \Delta V = \nabla \cdot \mathbf{j} \quad \text{in } \Omega_i, \quad (5)$$

$$[V]_{\Gamma_i} = 0 \quad \forall i \leq N, \quad (6)$$

$$[\sigma \partial_{\mathbf{n}_i} V]_{\Gamma_i} = 0 \quad \forall i \leq N, \quad (7)$$

where the symbol $[\cdot]_{\Gamma_i}$ denotes the jump of a function at the interface Γ_i , as defined in [35]. Boundary conditions (6) and (7) enforce the continuity of the potential and of the current across compartments.

The problem described by (5)-(7) can be recast as an integral equation. One such integral equation is the symmetric formulation, which is derived by exploiting the representation theorem [39, Theorem 3.1.1] and expressing the complete solution V as the sum of an homogeneous solution accounting for the source term and an harmonic function chosen to satisfy the boundary conditions (6) and (7). The homogeneous solution in free space can be obtained by application of the potential theory. Let

$$G(\mathbf{r}, \mathbf{r}') := \frac{1}{4\pi|\mathbf{r} - \mathbf{r}'|} \quad (8)$$

be the Green's function associated with the Laplace equation [22] [59, Equation 5.7], then $v(\mathbf{r}) = - \int (\nabla \cdot \mathbf{j}(\mathbf{r})) G(\mathbf{r}, \mathbf{r}') d\mathbf{r}'$ satisfies $\Delta v = \nabla \cdot \mathbf{j}$ for all $\mathbf{r} \in \mathbb{R}^3$. Following [35], we define then the piecewise source function $f_{\Omega_i}(\mathbf{r}) := (\nabla \cdot \mathbf{j}(\mathbf{r})) \cdot I_{\Omega_i}(\mathbf{r})$ and introduce

$$v_{\Omega_i}(\mathbf{r}) := - \int_{\Omega_i} f_{\Omega_i}(\mathbf{r}') G(\mathbf{r}, \mathbf{r}') d\mathbf{r}'. \quad (9)$$

In the symmetric formulation, the harmonic function is constructed as

$$u_{\Omega_i} := \begin{cases} V - \frac{v_{\Omega_i}}{\sigma_i} & \text{in } \Omega_i, \\ -\frac{v_{\Omega_i}}{\sigma_i} & \text{elsewhere,} \end{cases} \quad (10)$$

from which a system of $2N$ integral equations can be derived (see [35] for further details), reading

$$\begin{cases} (\partial_{\mathbf{n}} v_{\Omega_{i+1}})_{\Gamma_i} - (\partial_{\mathbf{n}} v_{\Omega_i})_{\Gamma_i} & = -\mathcal{D}_{i,i-1}^* p_{i-1} + 2\mathcal{D}_{ii}^* p_i - \mathcal{D}_{i,i+1}^* p_{i+1} \\ & \quad + \sigma_i \mathcal{N}_{i,i-1} V_{i-1} - (\sigma_i + \sigma_{i+1}) \mathcal{N}_{ii} V_i + \sigma_{i+1} \mathcal{N}_{i,i+1} V_{i+1} \\ \sigma_{i+1}^{-1} (v_{\Omega_{i+1}})_{\Gamma_i} - \sigma_i^{-1} (v_{\Omega_i})_{\Gamma_i} & = \mathcal{D}_{i,i-1} V_{i-1} - 2\mathcal{D}_{ii} V_i + \mathcal{D}_{i,i+1} V_{i+1} \\ & \quad - \sigma_i^{-1} \mathcal{S}_{i,i-1} p_{i-1} + (\sigma_i^{-1} + \sigma_{i+1}^{-1}) \mathcal{S}_{ii} p_i - \sigma_{i+1}^{-1} \mathcal{S}_{i,i+1} p_{i+1}. \end{cases} \quad (11)$$

The unknowns of the system are $V_i := (V)_{\Gamma_i}$, denoting the restriction of V to Γ_i , and $p_i := \sigma_i[\partial_{\mathbf{n}_i} V]_{\Gamma_i}$. The integral operators involved in equations (11) are defined as

$$\mathcal{S}_{ij} : H^{-1/2}(\Gamma_i) \rightarrow H^{1/2}(\Gamma_j), \quad \mathcal{S}_{ij}\psi(\mathbf{r}) := \int_{\Gamma_j} G(\mathbf{r} - \mathbf{r}')\psi(\mathbf{r}')dS(\mathbf{r}') \quad (12)$$

$$\mathcal{D}_{ij} : H^{1/2}(\Gamma_i) \rightarrow H^{1/2}(\Gamma_j), \quad \mathcal{D}_{ij}\phi(\mathbf{r}) := \text{p.v.} \int_{\Gamma_j} \partial_{\mathbf{n}'_i} G(\mathbf{r} - \mathbf{r}')\phi(\mathbf{r}')dS(\mathbf{r}') \quad (13)$$

$$\mathcal{D}_{ij}^* : H^{-1/2}(\Gamma_i) \rightarrow H^{-1/2}(\Gamma_j), \quad \mathcal{D}_{ij}^*\psi(\mathbf{r}) := \text{p.v.} \int_{\Gamma_j} \partial_{\mathbf{n}_j} G(\mathbf{r} - \mathbf{r}')\psi(\mathbf{r}')dS(\mathbf{r}') \quad (14)$$

$$\mathcal{N}_{ij} : H^{1/2}(\Gamma_i) \rightarrow H^{-1/2}(\Gamma_j), \quad \mathcal{N}_{ij}\phi(\mathbf{r}) := \text{f.p.} \int_{\Gamma_j} \partial_{\mathbf{n}_j} \partial_{\mathbf{n}'_i} G(\mathbf{r} - \mathbf{r}')\phi(\mathbf{r}')dS(\mathbf{r}') \quad (15)$$

and are respectively named single-layer, double-layer, adjoint double-layer, and hypersingular operators. The definition of the Sobolev spaces H^s , $s \in \{-1/2, 1/2\}$, in the mapping properties above can be found in [59, 52]. In the equations above, p.v. and f.p. indicate the Cauchy principal value and the Hadamard finite part. The subscript ij denotes that these operators act on a function defined on Γ_i and yield a function on Γ_j ; if this subscript is omitted, $i = j$ is implicitly assumed.

2.3. Discretization of the symmetric formulation

We employ the BEM to discretize and numerically solve the system of equations (11). To this end, a mesher triangulates the surfaces Γ_i resulting in a set of N meshes $\Gamma_{h,i}$, $i = 1, \dots, N$. In the following, the h subscript will be omitted in the case its meaning is already clear from the context. Each $\Gamma_{h,i}$ is composed of $N_{C,i}$ triangular cells, $\{c_{i,n}\}_{n=1}^{N_{C,i}}$, of area $A_{i,n}$, and $N_{V,i}$ vertices, $\{v_{i,m}\}_{m=1}^{N_{V,i}}$, and is characterized by the mesh refinement parameter h_i that is defined as the average length of the edges of $\Gamma_{h,i}$. Over each $\Gamma_{h,i}$, we define a set of piecewise constant $\{\pi_{i,n}\}_{n=1}^{N_{C,i}}$ patch functions and a set of piecewise linear $\{\lambda_{i,m}\}_{m=1}^{N_{V,i}}$ pyramid functions as

$$\pi_{i,n}(\mathbf{r}) := \begin{cases} 1 & \text{for } \mathbf{r} \in c_{i,n}, \\ 0 & \text{elsewhere,} \end{cases} \quad \text{and} \quad \lambda_{i,m}(\mathbf{r}) := \begin{cases} 1 & \text{for } \mathbf{r} = v_{i,m}, \\ 0 & \text{for } \mathbf{r} = v_{i,p \neq m}, \\ \text{linear} & \text{elsewhere.} \end{cases} \quad (16)$$

For the boundary element spaces spanned by these functions, $X_{\pi_i} := \text{span}\{\pi_{i,n}\}_{n=1}^{N_{C,i}}$ and $X_{\lambda_i} := \text{span}\{\lambda_{i,m}\}_{m=1}^{N_{V,i}}$, we have $X_{\pi_i} \subset H^{-1/2}(\Gamma_{h,i})$, $X_{\lambda_i} \subset H^{1/2}(\Gamma_{h,i})$ [59].

Following the standard Galerkin procedure, we expand the unknowns of the system in (11) as

$$V_i \approx \sum_{m=1}^{N_{V,i}} l_{i,m} \lambda_{i,m} \quad \text{and} \quad p_i \approx \sum_{n=1}^{N_{C,i}} p_{i,n} \pi_{i,n} \quad (17)$$

and we test with pyramid and patch functions resulting in the linear system of equations

$$\mathbf{Z} \begin{pmatrix} \mathbf{l} \\ \mathbf{p} \end{pmatrix} = \begin{pmatrix} \mathbf{b} \\ \mathbf{c} \end{pmatrix}. \quad (18)$$

The block matrix \mathbf{Z} can be represented as

$$\mathbf{Z} = \begin{pmatrix} \mathbf{N} & \mathbf{D}^* \\ \mathbf{D} & \mathbf{S} \end{pmatrix}, \quad (19)$$

where each block is another block matrix composed out of N^2 blocks, whose position inside $\{\mathbf{N}, \mathbf{D}^*, \mathbf{D}, \mathbf{S}\}$ will be identified by a block row index and a block column index. By denoting the blocks of $\{\mathbf{N}, \mathbf{D}^*, \mathbf{D}, \mathbf{S}\}$ in block row x

and block column y , for $x, y = 1, \dots, N$, with the superscript xy , their definitions are

$$\mathbf{N}^{xy} := \begin{cases} (\sigma_x + \sigma_{x+1})\mathbf{N}_{xy} & \text{if } x = y \\ -\sigma_y\mathbf{N}_{xy} & \text{if } x = y - 1 \\ -\sigma_x\mathbf{N}_{xy} & \text{if } x = y + 1 \\ 0 \cdot \mathbf{N}_{xy} & \text{otherwise} \end{cases}, \quad \mathbf{D}^{*xy} := \begin{cases} -2\mathbf{D}_{xy}^* & \text{if } x = y \\ \mathbf{D}_{xy}^* & \text{if } x = y \pm 1 \\ 0 \cdot \mathbf{D}_{xy}^* & \text{otherwise} \end{cases},$$

$$\mathbf{D}^{xy} := \begin{cases} -2\mathbf{D}_{xy} & \text{if } x = y \\ \mathbf{D}_{xy} & \text{if } x = y \pm 1 \\ 0 \cdot \mathbf{D}_{xy} & \text{otherwise} \end{cases}, \quad \mathbf{S}^{xy} := \begin{cases} (\sigma_x^{-1} + \sigma_{x+1}^{-1})\mathbf{S}_{xy} & \text{if } x = y \\ -\sigma_y^{-1}\mathbf{S}_{xy} & \text{if } x = y - 1 \\ -\sigma_x^{-1}\mathbf{S}_{xy} & \text{if } x = y + 1 \\ 0 \cdot \mathbf{S}_{xy} & \text{otherwise} \end{cases}.$$

The matrices introduced in the previous equations are defined as

$$(\mathbf{N}_{xy})_{mn} := (\lambda_{x,m}, \mathbf{N}_{xy}\lambda_{y,n})_{L^2(\Gamma_x)}, \quad (20)$$

$$(\mathbf{D}_{xy}^*)_{mn} := (\lambda_{x,m}, \mathcal{D}_{xy}^*\pi_{y,n})_{L^2(\Gamma_x)}, \quad (21)$$

$$(\mathbf{D}_{xy})_{mn} := (\pi_{x,m}, \mathcal{D}_{xy}\lambda_{y,n})_{L^2(\Gamma_x)}, \quad (22)$$

$$(\mathbf{S}_{xy})_{mn} := (\pi_{x,m}, \mathcal{S}_{xy}\pi_{y,n})_{L^2(\Gamma_x)}. \quad (23)$$

The blocks of the right-hand-side (RHS) vector in equation (18) can be written as

$$\mathbf{b} = \begin{pmatrix} \mathbf{b}_1 \\ \mathbf{b}_2 \\ \vdots \\ \mathbf{b}_N \end{pmatrix}, \quad \mathbf{c} = \begin{pmatrix} \mathbf{c}_1 \\ \mathbf{c}_2 \\ \vdots \\ \mathbf{c}_N \end{pmatrix}, \quad (24)$$

where

$$(\mathbf{b}_i)_m := (\lambda_{i,m}, (\partial_{\mathbf{n}}v_{\Omega_{i+1}} - \partial_{\mathbf{n}}v_{\Omega_i}))_{L^2(\Gamma_i)}, \quad (25)$$

$$(\mathbf{c}_i)_n := (\pi_{i,n}, (\sigma_{i+1}^{-1}v_{\Omega_{i+1}} - \sigma_i^{-1}v_{\Omega_i}))_{L^2(\Gamma_i)}. \quad (26)$$

The blocks of the unknown vector in equation (18) can be written as

$$\mathbf{l} = \begin{pmatrix} \mathbf{l}_1 \\ \mathbf{l}_2 \\ \vdots \\ \mathbf{l}_N \end{pmatrix}, \quad \mathbf{p} = \begin{pmatrix} \mathbf{p}_1 \\ \mathbf{p}_2 \\ \vdots \\ \mathbf{p}_N \end{pmatrix}, \quad (27)$$

whose elements are simply $(\mathbf{l}_i)_m := l_{i,m}$ and $(\mathbf{p}_i)_n := p_{i,n}$. The elements of \mathbf{l}_i are the voltages at the vertices of $\Gamma_{h,i}$ due to the interpolatory nature of the basis functions. As a final remark, the last block-row and the last block-column of the linear system in (18) need to be eliminated [35], as the exterior conductivity σ_{N+1} is null.

2.4. Operators and dual basis functions needed for the new formulation

This section establishes further operators and basis functions needed for the new formulation. First, we barycentrically refine $\Gamma_{h,i}$ resulting in $\bar{\Gamma}_{h,i}$. Using $\bar{\Gamma}_{h,i}$ we obtain the dual mesh $\tilde{\Gamma}_{h,i}$, where the vertices of $\Gamma_{h,i}$ have become cells and the cells of $\Gamma_{h,i}$ have become vertices (see Figure 1). On $\tilde{\Gamma}_{h,i}$, we define dual pyramid basis functions $\tilde{\lambda}_{i,n}$, which are attached to the dual vertices $\tilde{v}_{i,n}$, defined by

$$\tilde{\lambda}_{i,n}(\mathbf{r}) := \sum_{x=1}^7 \frac{1}{\text{NoC}(\tilde{v}_{i,n,x})} \bar{\lambda}_{i,n,x}(\mathbf{r}), \quad (28)$$

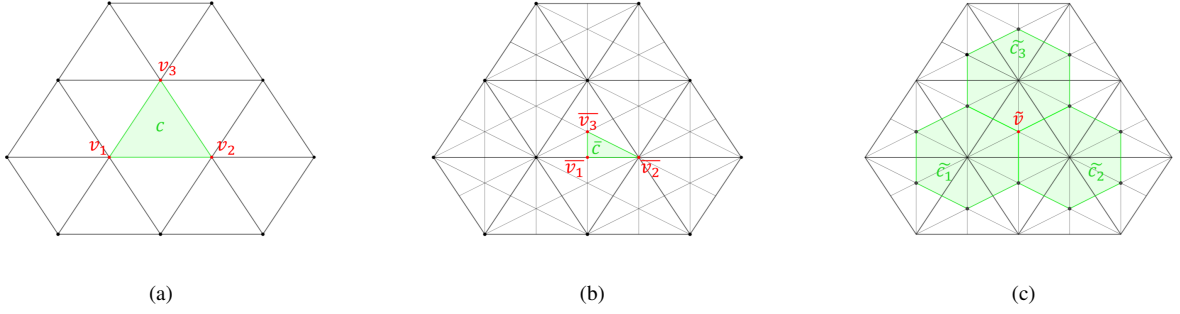


Fig. 1. (a) Primal, (b) barycentrically refined, and (c) dual mesh, denoted respectively as $\Gamma_{h,i}$, $\bar{\Gamma}_{h,i}$, and $\tilde{\Gamma}_{h,i}$. The vertices are in red, the cells are in green.

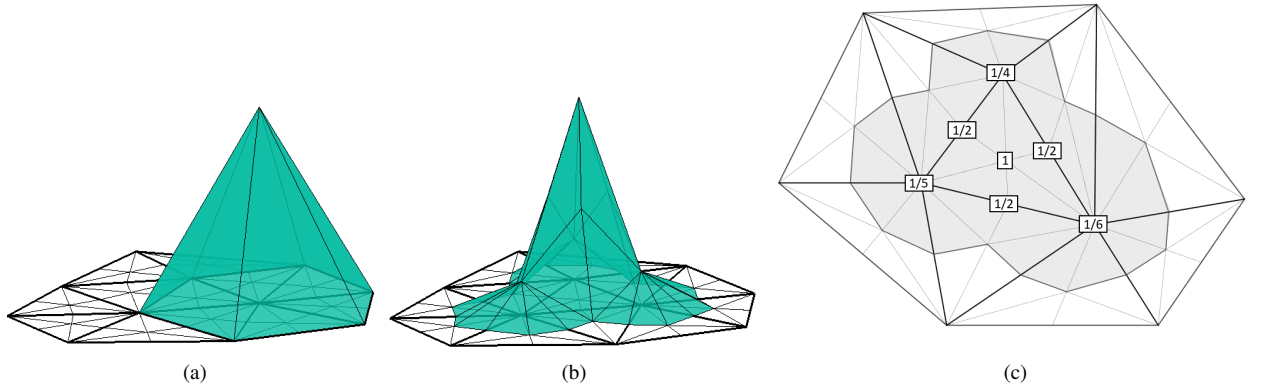


Fig. 2. (a) Primal and (b) dual pyramid basis function representation. (c) Dual pyramid basis function support: the numbers denote the value of the function at the point.

where $\bar{\lambda}_{i,n,x}$ is the pyramid function with domain on the barycentrically refined mesh $\bar{\Gamma}_{h,i}$, attached to the x th vertex of $\bar{\Gamma}_{h,i}$, $\{\bar{v}_{i,n,x}\}_{x=1}^7$, lying on the primal cell $c_{i,n}$, and the function $NoC(\bar{v}_{i,n,x})$ gives the number of primal cells connected to the vertex $\bar{v}_{i,n,x}$. A graphical representation of the dual pyramid basis function is shown in Figure 2b.

In the following, we will also need the identity \mathcal{I} and the Laplace-Beltrami Δ_{Γ_i} operators. They can be discretized through their application to a given set of expansion functions and the testing with a set of test basis functions. For the identity operator, the outcome of this operation is usually named Gram matrix, denoted in this work by $\mathbf{G}_{i,f,g}$, where $f, g \in \{\pi, \lambda, \tilde{\lambda}\}$ indicate the type of test and expansion functions employed in the discretization

$$(\mathbf{G}_{i,f,g})_{mn} := (f_{i,m}(\mathbf{r}), g_{i,n}(\mathbf{r}))_{L^2(\Gamma_i)}. \tag{29}$$

The discretization of the Laplace-Beltrami operator by means of pyramid and dual pyramid functions leads to the matrices

$$(\mathbf{\Delta}_i)_{mn} := (\nabla_{\Gamma_i} \lambda_{i,m}, \nabla_{\Gamma_i} \lambda_{i,n})_{L^2(\Gamma_i)}, \tag{30}$$

$$(\tilde{\mathbf{\Delta}}_i)_{mn} := (\nabla_{\Gamma_i} \tilde{\lambda}_{i,m}, \nabla_{\Gamma_i} \tilde{\lambda}_{i,n})_{L^2(\Gamma_i)}, \tag{31}$$

where ∇_{Γ_i} denotes the surface gradient operator [52, Equation 4.200]. The constant function along Γ_i , $I(\mathbf{r}) := 1$, is an eigensolution of the Laplace-Beltrami operator, that is $\Delta_{\Gamma_i} I = 0$. Hence, the one-dimensional nullspace of the Laplace-Beltrami operator is spanned by the constant function, in symbols $\ker \Delta_{\Gamma_i} = \text{span}\{I\}$. Due to our choice of basis and test functions, $\mathbf{\Delta}_i$ and $\tilde{\mathbf{\Delta}}_i$ have, likewise, a non-trivial nullspace given by $\mathbf{1}_{N_{v,i}}$ and $\mathbf{1}_{N_{c,i}}$, where $\mathbf{1}_n$ denotes the all-one vector in \mathbb{R}^n .

3. Analysis of the conditioning of the symmetric formulation

The ill-conditioning plaguing the symmetric formulation can be traced back to two distinct numerical effects: the dense-discretization breakdown (i.e., the increase of the condition number for $h \rightarrow 0$, where $h := \min_i h_i$) and the high-contrast breakdown (i.e. the increase of the condition number for an increasing conductivity contrast between adjacent compartments).

The stability analysis proposed here aims at characterizing the discrete spectral behaviour of the formulation, in particular through the estimation of the condition number of \mathbf{Z} [47, Equation 2.1.25], $\text{cond}(\mathbf{Z})$, given by the ratio between the highest and the lowest singular values of \mathbf{Z} which is known to impact, for most iterative solvers, both the speed of convergence and the achievable accuracy (in finite precision arithmetic) [47].

3.1. Dense-discretization behaviour

In this section, we will study the stability properties of the discrete symmetric formulation when h decreases. We base our analysis on the spherical harmonics decomposition of the operator; thus, we employ a spherical multi-compartment head model. We do not loose generality here, as realistic multi-compartment head models will have similar spectral properties since a smooth deformation of a geometry gives rise to a compact perturbation of the electrostatic operators under study [56, 34]. The assumption of a smooth deformation is uncritical as human heads typically do not have sharp edges and corners.

We consider an head model characterized by N concentric, spherical boundaries $\{\Gamma_i\}_{i=1}^N$ with radius $\{R_i\}_{i=1}^N$. The operator under study

$$\mathbf{Z} = \begin{pmatrix} \mathcal{N}_b & \mathcal{D}_b^* \\ \mathcal{D}_b & \mathcal{S}_b \end{pmatrix} \quad (32)$$

is a block integral operator, where each block operator is another block operator composed of N^2 blocks. By denoting the operator in block row x and block column y of $\{\mathcal{N}_b, \mathcal{D}_b^*, \mathcal{D}_b, \mathcal{S}_b\}$, for $x, y = 1, \dots, N$, with the superscript xy , we have

$$\mathcal{N}_b^{xy} := \begin{cases} (\sigma_x + \sigma_{x+1})\mathcal{N}_{xy} & \text{if } x = y \\ -\sigma_y\mathcal{N}_{xy} & \text{if } x = y - 1 \\ -\sigma_x\mathcal{N}_{xy} & \text{if } x = y + 1 \\ 0 \cdot \mathcal{N}_{xy} & \text{otherwise} \end{cases} \quad \mathcal{D}_b^{*xy} := \begin{cases} -2\mathcal{D}_{xy}^* & \text{if } x = y \\ \mathcal{D}_{xy}^* & \text{if } x = y \pm 1 \\ 0 \cdot \mathcal{D}_{xy}^* & \text{otherwise} \end{cases}$$

$$\mathcal{D}_b^{xy} := \begin{cases} -2\mathcal{D}_{xy} & \text{if } x = y \\ \mathcal{D}_{xy} & \text{if } x = y \pm 1 \\ 0 \cdot \mathcal{D}_{xy} & \text{otherwise} \end{cases} \quad \mathcal{S}_b^{xy} := \begin{cases} (\sigma_x^{-1} + \sigma_{x+1}^{-1})\mathcal{S}_{xy} & \text{if } x = y \\ -\sigma_y^{-1}\mathcal{S}_{xy} & \text{if } x = y - 1 \\ -\sigma_x^{-1}\mathcal{S}_{xy} & \text{if } x = y + 1 \\ 0 \cdot \mathcal{S}_{xy} & \text{otherwise} \end{cases}$$

We begin our analysis by noting that due to the compactness of the double-layer operator \mathcal{D}_{xy} (13) and its adjoint counterpart \mathcal{D}_{xy}^* (14) on smooth domains [17], the blocks $\mathcal{D}_b, \mathcal{D}_b^*$ are block operators, where each block is a compact operator; hence, $\mathcal{D}_b, \mathcal{D}_b^*$ are compact (see Appendix A for a proof). Moreover, the single-layer $\mathcal{S}_{i,j \neq i}$ (12) and the hypersingular operators $\mathcal{N}_{i,j \neq i}$ (15) are compact as their kernels are continuous provided the analyticity of the Green's function evaluated in \mathbf{r} far enough from \mathbf{r}' [52, Chapter 5.1.3], [16, Theorem 1.10]. Finally, the operator \mathbf{Z} can be decomposed into the sum of a block operator involving only its diagonal blocks and another block operator, $\mathcal{K}_{\mathbf{Z}}$, containing the off-diagonal, compact contributions,

$$\mathbf{Z} = \text{diag} \left((\sigma_1 + \sigma_2)\mathcal{N}_{11}, (\sigma_2 + \sigma_3)\mathcal{N}_{22}, \dots, (\sigma_N + \sigma_{N+1})\mathcal{N}_{NN}, \right. \\ \left. (\sigma_1^{-1} + \sigma_2^{-1})\mathcal{S}_{11}, (\sigma_2^{-1} + \sigma_3^{-1})\mathcal{S}_{22}, \dots, (\sigma_N^{-1} + \sigma_{N+1}^{-1})\mathcal{S}_{NN} \right) + \mathcal{K}_{\mathbf{Z}}. \quad (33)$$

The contribution $\mathcal{K}_{\mathbf{Z}}$, a block operator with compact blocks, is compact, as proved in Appendix A. Since its eigenvalues accumulate at zero when increasing the number of degrees of freedom of the problem [16, Theorem 1.34], the dominant spectral properties of \mathbf{Z} are determined by the ones of the first, non-compact, operator in the summation (33). Therefore, we have to study the eigenvalues of the first term in (33), given by the union of the sets of eigenvalues of each diagonal block. We obtain those eigenvalues by noting that the spherical harmonic function Y_{lm} of degree l

and order m with $l \geq 0$ and $|m| < l$ (for a formal definition, see [40, Definition 14.30.1]) is an eigenfunction of the single-layer and the hypersingular operator [31]

$$\mathcal{S}_{ii}Y_{lm} = \lambda_{l,S_{ii}}Y_{lm}, \quad (34)$$

$$\mathcal{N}_{ii}Y_{lm} = \lambda_{l,N_{ii}}Y_{lm}, \quad (35)$$

where the eigenvalues of the previous equations are

$$\lambda_{l,S_{ii}} = \frac{R_i}{2l+1}, \quad \text{with multiplicity } 2l+1 \quad (36)$$

$$\lambda_{l,N_{ii}} = -\frac{l(l+1)}{R_i(2l+1)}, \quad \text{with multiplicity } 2l+1. \quad (37)$$

Due to the definiteness property of the self-adjoint operators \mathcal{S}_{ii} , \mathcal{N}_{ii} , their singular values are simply obtained as $\sigma_{l,S_{ii}} = \lambda_{l,S_{ii}}$ and $\sigma_{l,N_{ii}} = -\lambda_{l,N_{ii}}$.

The resulting set of eigenvalues of $(\mathcal{Z} - \mathcal{K}_{\mathcal{Z}})$ reads

$$\begin{aligned} \text{eig}(\mathcal{Z} - \mathcal{K}_{\mathcal{Z}}) = & \{(\sigma_1 + \sigma_2)\lambda_{l,N_{11}}, (\sigma_2 + \sigma_3)\lambda_{l,N_{22}}, \dots, (\sigma_l + \sigma_{l+1})\lambda_{l,N_{NN}}\} \cup \\ & \{(\sigma_1^{-1} + \sigma_2^{-1})\lambda_{l,S_{11}}, (\sigma_2^{-1} + \sigma_3^{-1})\lambda_{l,S_{22}}, \dots, (\sigma_{N-1}^{-1} + \sigma_N^{-1})\lambda_{l,S_{N-1,N-1}}\}. \end{aligned} \quad (38)$$

Hence, we can recognize different branches of eigenvalues of $(\mathcal{Z} - \mathcal{K}_{\mathcal{Z}})$: on one side, those associated to \mathcal{N}_{ii} , $(\sigma_i + \sigma_{i+1})\lambda_{l,N_{ii}}$, diverging towards minus infinity with the order l of the corresponding eigenfunction, and, on the other side, those associated to \mathcal{S}_{ii} , $(\sigma_i^{-1} + \sigma_{i+1}^{-1})\lambda_{l,S_{ii}}$, converging toward 0 for $l \rightarrow \infty$.

To obtain a statement on how the condition number grows in h_i , we note that the maximum degree l supported by a mesh resolution h_i behaves asymptotically as $l = \mathcal{O}(R_i h_i^{-1})$ [3]. We then find

$$\sigma_{l,N_{ii}} = -\lambda_{l,N_{ii}} = \mathcal{O}(R_i^{-1}l) = \mathcal{O}(h_i^{-1}), \quad (39)$$

$$\sigma_{l,S_{ii}} = \lambda_{l,S_{ii}} = \mathcal{O}(R_i l^{-1}) = \mathcal{O}(h_i), \quad (40)$$

showing the ill-conditioned nature of the symmetric formulation and resulting in a condition number growth of its discretization by means of an L^2 -orthonormal basis as $\mathcal{O}(h^{-2})$.

3.2. High-contrast behaviour

From the expression of the eigenvalues of $(\mathcal{Z} - \mathcal{K}_{\mathcal{Z}})$ on a spherical head model (38), another source of ill conditioning can be verified, related to the conductivity contrast between different compartments of the head domain Ω . We define the conductivity ratio between the adjacent compartments Ω_i and Ω_{i+1} as

$$CR_i := \frac{\max(\sigma_i, \sigma_{i+1})}{\min(\sigma_i, \sigma_{i+1})}, \quad (41)$$

and can see that the condition number grows with increasing CR_i by first considering that, asymptotically, $CR_i \rightarrow \infty$ corresponds either to the condition $(\sigma_i + \sigma_{i+1}) \rightarrow \infty$ when $\max(\sigma_i, \sigma_{i+1}) \rightarrow \infty$, or to $(\sigma_i^{-1} + \sigma_{i+1}^{-1}) \rightarrow 0$ when $\min(\sigma_i, \sigma_{i+1}) \rightarrow 0$. Then, the absolute difference between the branch of eigenvalues $(\sigma_i + \sigma_{i+1})\lambda_{l,N_{ii}}$ and the branch $(\sigma_i^{-1} + \sigma_{i+1}^{-1})\lambda_{l,S_{ii}}$ grows when increasing the parameter CR_i , leading to an increasing condition number. Therefore, we conclude that the instability of the symmetric formulation is worsened in presence of high-contrast models. The high-contrast behavior, together with the dense-discretization ill-conditioning outlined in the previous Section 3.1, actually places a limit on the effective use of the symmetric formulation applied to realistic scenarios, where the head model is characterized by high-contrasts between the skull and the nearby tissues and the meshes are heavily refined, in order to capture small anatomical details since high condition numbers can lead to slowly or non-converging iterative solvers.

4. The new formulation

The preconditioning strategy proposed in this work makes the symmetric formulation immune to both the dense-discretization and the high-contrast breakdowns. Differently from standard Calderón approaches, ours is obtained at continuous level through the product of three operators. To clarify the ideas, before introducing the complete formulation, we will consider the regularization of the single-layer operator only as a proof of concept.

4.1. A proof of concept

The single-layer operator $\mathcal{S}_{11} : H^{-1/2}(\Gamma_1) \rightarrow H^{1/2}(\Gamma_1)$, where Γ_1 is smooth, is a pseudo-differential operator of order -1 [60]. From its boundedness and $H^{-1/2}$ -ellipticity [59, Equation 6.8], it follows that, for any $f \in H^{1/2}(\Gamma_1)$, the solution of the equation $\mathcal{S}u = f$ is unique (Lax-Milgram theorem, [59, Theorem 3.4]). However, as can be seen from the spectral analysis in Section 3.1, this integral equation is first-kind in nature and its discretization gives rise to an ill-conditioned system of linear equations. As suggested in [60], a preconditioning operator for \mathcal{S} can be constructed by explicitly evaluating the inverse of the principal symbol of \mathcal{S} and by finding its associated self-adjoint, elliptic preconditioning operator, of pseudodifferential order 1. This strategy, better known as Calderón preconditioning, has a theoretical basis in the Calderón identity [39, Equation 3.1.45]

$$-\mathcal{N}\mathcal{S} = \frac{\mathcal{I}}{4} - \mathcal{D}^{*2}, \quad (42)$$

stating that the product of the hypersingular and the single-layer operator gives rise to a second kind operator.

Other possibilities exist, however. We consider for example the operator $\mathcal{S}_{11}\Delta_{\Gamma_1}\mathcal{S}_{11}$, where the Laplace-Beltrami operator $\Delta_{\Gamma_1} : H^\alpha(\Gamma_1) \rightarrow H^{\alpha-2}(\Gamma_1)$ is a pseudo-differential operator of order 2. The product $\mathcal{S}_{11}\Delta_{\Gamma_1} : H^{-1/2}(\Gamma_1) \rightarrow H^{-3/2}(\Gamma_1)$ satisfies the condition of being of order 1, so it could give rise to a suitable left preconditioner for \mathcal{S}_{11} . The favorable conditioning properties of $\mathcal{S}_{11}\Delta_{\Gamma_1}\mathcal{S}_{11}$ have been shown in [41], where, by explicit expansion of the product, $\mathcal{S}_{11}\Delta_{\Gamma_1}\mathcal{S}_{11}$ has been proved to be a second-kind integral operator, with its spectrum accumulating at $1/4$,

$$\mathcal{S}_{11}\Delta_{\Gamma_1}\mathcal{S}_{11} = \frac{\mathcal{I}}{4} + \mathcal{K}_{\mathcal{S}_{11}\Delta_{\Gamma_1}\mathcal{S}_{11}}, \quad (43)$$

where $\mathcal{K}_{\mathcal{S}_{11}\Delta_{\Gamma_1}\mathcal{S}_{11}}$ is compact. It follows that the matrix $\mathbf{G}_{1,\pi\pi}^{-1/2}\mathbf{S}_{11}\mathbf{G}_{1,\lambda\pi}^{-1}\tilde{\mathbf{A}}_1\mathbf{G}_{1,\lambda\pi}^{-1}\mathbf{S}_{11}\mathbf{G}_{1,\pi\pi}^{-1/2}$, discretizing the second kind operator $\mathcal{S}\Delta_{\Gamma_1}\mathcal{S}$ by means of an orthonormal set of basis functions, is well-conditioned up to its nullspace and its spectrum accumulates at the point $1/4$.

However, the discrete preconditioning presented above is in general not allowed, because of the one-dimensional nullspace of $\tilde{\mathbf{A}}_1$, which is spanned by the all-one vector. Indeed, the application of a singular preconditioner to a non-singular system of linear equations causes a loss of information which prevents recovering the solution of the original problem. To overcome this issue, following the approach presented in [60], we introduce the operator $\hat{\Delta}_{\Gamma_i} : H^\alpha(\Gamma_i) \rightarrow H^{\alpha-2}(\Gamma_i)$ defined by the bilinear form

$$\left(v, \hat{\Delta}_{\Gamma_i} w\right)_{L^2(\Gamma_i)} := \left(\nabla_{\Gamma_i} w, \nabla_{\Gamma_i} v\right)_{L^2(\Gamma_i)} + (I, w)_{L^2(\Gamma_i)} (I, v)_{L^2(\Gamma_i)}. \quad (44)$$

The operator $\hat{\Delta}_{\Gamma_i}$ is invertible. Therefore, the unique solution of the problem

$$\hat{\Delta}_{\Gamma_i} w = g \quad (45)$$

is also a solution of the ill-posed problem

$$\Delta_{\Gamma_i} w = g \quad (46)$$

if g satisfies the solvability condition $\int_{\Gamma_i} g dS = 0$. The discretizations of $\hat{\Delta}_{\Gamma_i}$ by means of pyramid functions defined on Γ_i ,

$$\hat{\mathbf{A}}_i := \mathbf{A}_i + \mathbf{G}_{i,\lambda\lambda}^T \mathbf{1}_{N_{V,i}} \mathbf{1}_{N_{V,i}}^T \mathbf{G}_{i,\lambda\lambda}, \quad (47)$$

and the one by means of dual pyramid functions defined on $\tilde{\Gamma}_i$,

$$\hat{\tilde{\mathbf{A}}}_i := \tilde{\mathbf{A}}_i + \mathbf{G}_{i,\tilde{\lambda}\tilde{\lambda}}^T \mathbf{1}_{N_{C,i}} \mathbf{1}_{N_{C,i}}^T \mathbf{G}_{i,\tilde{\lambda}\tilde{\lambda}}, \quad (48)$$

are non-singular matrices. As in the case of $\mathcal{S}_{11}\Delta_{\Gamma_1}\mathcal{S}_{11}$, it can be shown that $\mathcal{S}_{11}\hat{\Delta}_{\Gamma_1}\mathcal{S}_{11}$ is a second-kind integral operator accumulating at $1/4$. Indeed, by expanding its weak form, following the steps in [41], one obtains

$$\left(\mathcal{S}_{11}\hat{\Delta}_{\Gamma_1}\mathcal{S}_{11}v, w\right)_{L^2(\Gamma_1)} = \frac{1}{4}(v, w)_{L^2(\Gamma_1)} + \left(\mathcal{K}_{\mathcal{S}_{11}\Delta_{\Gamma_1}\mathcal{S}_{11}}v, w\right)_{L^2(\Gamma_1)} - (I, \mathcal{S}_{11}v)_{L^2(\Gamma_1)}(I, w)_{L^2(\Gamma_1)}. \quad (49)$$

Since the term $(I, \mathcal{S}_{11}v)_{L^2(\Gamma_i)}(I, w)_{L^2(\Gamma_i)}$ represents the bilinear form of a separable operator with finite dimensional range, $\mathcal{S}_{11}\hat{\Delta}_{\Gamma_i}\mathcal{S}_{11}$ is a second-kind operator and its strong form can be written as

$$\mathcal{S}_{11}\hat{\Delta}_{\Gamma_i}\mathcal{S}_{11} = \frac{I}{4} + \mathcal{K}_{\mathcal{S}_{11}\hat{\Delta}_{\Gamma_i}\mathcal{S}_{11}}, \quad (50)$$

where $\mathcal{K}_{\mathcal{S}_{11}\hat{\Delta}_{\Gamma_i}\mathcal{S}_{11}}$ is compact. Thus, given $f \in H^{1/2}(\Gamma_i)$ and the vector of coefficients of its linear expansion in patch basis function \mathbf{f} , the system of linear equations

$$\mathcal{S}_{11}\mathbf{G}_{1,\tilde{\lambda}\pi}^{-1}\hat{\Delta}_1\mathbf{G}_{1,\tilde{\lambda}\pi}^{-1}\mathcal{S}_{11}\mathbf{x} = \mathcal{S}_{11}\mathbf{G}_{1,\tilde{\lambda}\pi}^{-1}\hat{\Delta}_1\mathbf{G}_{1,\tilde{\lambda}\pi}^{-1}\mathbf{f} \quad (51)$$

is non-singular and well-conditioned. Its unique solution coincides with the solution of the non-singular, but ill-conditioned, original problem $\mathcal{S}_{11}\mathbf{x} = \mathbf{f}$.

4.2. A non-singular symmetric formulation

As well-known from the literature [35], when the conductivity in Ω_{N+1} (the exterior region) is zero, as is customary in EEG scenarios, the symmetric formulation is not well-posed due to a one-dimensional nullspace. This characteristic reflects the indeterminacy of the electrostatic potential, defined from the relation $\mathbf{E} = -\nabla V$ up to a constant [35]. Specifically, we find the one-dimensional, non-trivial nullspace of matrix \mathbf{Z} as the direction parallel to

$$\ker(\mathbf{Z}) = \left[\mathbf{1}_{N_{V,1}}^T \quad \mathbf{1}_{N_{V,2}}^T \quad \dots \quad \mathbf{1}_{N_{V,N}}^T \quad \mathbf{0}_{N_{C,1}}^T \quad \mathbf{0}_{N_{C,2}}^T \quad \dots \quad \mathbf{0}_{N_{C,N-1}}^T \right]^T, \quad (52)$$

following from

$$\begin{cases} \mathbf{N}_{ij}\mathbf{1}_{N_{V,j}} &= \mathbf{0}_{N_{V,i}}, \\ \mathcal{D}_{i-1,i}\mathbf{1}_{N_{V,i}} &= -\mathbf{G}_{\pi\pi,i-1}\mathbf{1}_{N_{C,i-1}}, \\ \mathcal{D}_{ii}\mathbf{1}_{N_{V,i}} &= -\frac{1}{2}\mathbf{G}_{\pi\pi,i}\mathbf{1}_{N_{C,i}}, \\ \mathcal{D}_{i+1,i}\mathbf{1}_{N_{V,i}} &= \mathbf{0}_{N_{C,i+1}}, \end{cases} \quad (53)$$

which are the discrete counterparts of the eigenrelations

$$\begin{cases} \mathcal{N}_{ij}I &= 0 \\ \mathcal{D}_{i-1,i}I &= -I, \\ \mathcal{D}_{ii}I &= -\frac{1}{2}I, \\ \mathcal{D}_{i+1,i}I &= 0. \end{cases} \quad (54)$$

The first relation of system (53) identifies the non-trivial kernel of matrix \mathbf{N}_{ij} discretizing the hypersingular operator applied to a function expanded in an interpolatory basis. The three last equations of (54) follow instead from a direct application of the representation theorem [39, Theorem 3.1.1]. Their validity can be shown for example by applying the representation formula in [39, Equation 3.1.7] to the scalar function $u(\mathbf{r})$, defined as constant in the interior of Γ_i and null elsewhere.

A deflation strategy is needed to obtain a non-singular problem (i.e., admitting unique solution), whose application is physically equivalent to fixing a reference for the evaluation of the potential. To the purpose of its implementation, similarly to what done in the previous section, we define the operator $\hat{\mathcal{N}}_{ii} : H^{1/2}(\Gamma_i) \rightarrow H^{-1/2}(\Gamma_i)$ [60] by the bilinear form

$$(\hat{\mathcal{N}}_{ii}v, w)_{L^2(\Gamma_i)} := (\mathcal{N}_{ii}v, w)_{L^2(\Gamma_i)} + (I, w)_{L^2(\Gamma_i)}(I, v)_{L^2(\Gamma_i)} \quad (55)$$

for all $v, w \in H^{1/2}(\Gamma_i)$. This modified hypersingular operator is bounded and $H^{1/2}$ -elliptic [59]. Moreover, the unique solution of

$$\hat{\mathcal{N}}_{ii}v = g \quad (56)$$

is also a solution of

$$\mathcal{N}_{ii}v = g, \quad (57)$$

provided that the solvability condition $\int_{\Gamma_i} g dS = 0$ is satisfied. The discretization of $\hat{\mathcal{N}}_{ii}$ with pyramid functions as testing and expansion functions on Γ_i gives rise to the invertible matrix

$$\hat{\mathbf{N}}_{ii} := \mathbf{N}_{ii} + \mathbf{G}_{i,\lambda\lambda}^T \mathbf{1}_{N_{V,i}} \mathbf{1}_{N_{V,i}}^T \mathbf{G}_{i,\lambda\lambda}. \quad (58)$$

Among the infinite deflation choices available, one of them allows to retrieve the solution corresponding to a mean-value free potential on the exterior layer, a favorable choice in terms of compatibility with the most common measurement setups [36] and based on theoretical justifications [12]. This is simply obtained by using $\hat{\mathbf{N}}_{NN}$ instead of \mathbf{N}_{NN} . Equivalently, by defining the vector

$$\boldsymbol{\zeta} := \left[\mathbf{0}_{N_{V,1}}^T \quad \mathbf{0}_{N_{V,2}}^T \quad \dots \quad \mathbf{G}_{N,\lambda\lambda}^T \mathbf{1}_{N_{V,N}} \quad \mathbf{0}_{N_{C,1}}^T \quad \dots \quad \mathbf{0}_{N_{C,N-1}}^T \right]^T, \quad (59)$$

the unique solution of the linear system of equations

$$\hat{\mathbf{Z}} \begin{pmatrix} l \\ \rho \end{pmatrix} = (\mathbf{Z} + \boldsymbol{\zeta} \boldsymbol{\zeta}^T) \begin{pmatrix} l \\ \rho \end{pmatrix} = \begin{pmatrix} b \\ c \end{pmatrix} \quad (60)$$

is also a solution of

$$\mathbf{Z} \begin{pmatrix} l \\ \rho \end{pmatrix} = \begin{pmatrix} b \\ c \end{pmatrix}. \quad (61)$$

Moreover, V_N is a mean-value free function, that is, we have

$$(\mathbf{G}_{N,\lambda\lambda}^T \mathbf{1}_N)^T \mathbf{1}_{N_{V,N}} = 0. \quad (62)$$

The above statements follow from the existence of a solution of equation (61) satisfying condition (62) and from the uniqueness of the solution of equation (60). In the next section, we will define a preconditioning strategy for the well-posed formulation in (60).

4.3. Our preconditioned, non-singular symmetric formulation

The new formulation, resulting from the preconditioning of (60), for which we are going to prove the good conditioning properties, reads

$$\mathbf{Z}_p \mathbf{y} := \mathbf{M} \mathbf{Q} \hat{\mathbf{Z}} \mathbf{Q} \mathbf{G} \mathbf{P} \mathbf{G}^T \mathbf{Q} \hat{\mathbf{Z}} \mathbf{Q} \mathbf{M} \mathbf{y} = \mathbf{M} \mathbf{Q} \hat{\mathbf{Z}} \mathbf{Q} \mathbf{G} \mathbf{P} \mathbf{G}^T \mathbf{Q} \begin{pmatrix} b \\ c \end{pmatrix}. \quad (63)$$

The solution of the original problem (60) is retrieved as

$$\begin{pmatrix} l \\ \rho \end{pmatrix} = \mathbf{Q} \mathbf{M} \mathbf{y}. \quad (64)$$

In the following, the matrices in (63) and a brief, intuitive explanation of their use in the formulation are introduced. The rigorous proof of the well conditioning of the formulation will be given in the next section.

The matrix \mathbf{Q} is defined as

$$\mathbf{Q} := \text{diag} \left(q_{V,1} \sqrt{R_1} \cdot \mathbf{I}_{N_{V,1},N_{V,1}}, q_{V,2} \sqrt{R_2} \cdot \mathbf{I}_{N_{V,2},N_{V,2}}, \dots, q_{V,N} \sqrt{R_N} \cdot \mathbf{I}_{N_{V,N},N_{V,N}}, \right. \\ \left. \frac{q_{C,1}}{\sqrt{R_1}} \cdot \mathbf{I}_{N_{C,1},N_{C,1}}, \frac{q_{C,2}}{\sqrt{R_2}} \cdot \mathbf{I}_{N_{C,2},N_{C,2}}, \dots, \frac{q_{C,N-1}}{\sqrt{R_{N-1}}} \cdot \mathbf{I}_{N_{C,N-1},N_{C,N-1}} \right), \quad (65)$$

where $\mathbf{I}_{nm} \in \mathbb{R}^{n \times m}$ denotes the generalized (rectangular) identity matrix, i.e. $(\mathbf{I}_{nm})_{xy} = \delta_{xy}$, with δ_{xy} the Kronecker delta function. The scalar coefficients $q_{V,i}$, $q_{C,i}$ are defined as [42]

$$q_{V,i} := \max(\sigma_i, \sigma_{i+1})^{-1/2} \quad (66)$$

$$q_{C,i} := \min(\sigma_i, \sigma_{i+1})^{1/2} \quad (67)$$

and have been introduced in the formulation in order to cure the high-contrast breakdown identified in Section 3.2. Indeed, as shown in [42], the left and right multiplication of $\hat{\mathbf{Z}}$ by \mathbf{Q} makes the symmetric formulation immune to this source of ill-conditioning.

If $\Gamma_{h,i}$ discretizes a spherical surface, then we define R_i as the radius of the approximating sphere. Otherwise, R_i represents half of the characteristic length of the inner volume delimited by Γ_i .

The matrix \mathbf{P}

$$\mathbf{P} := \text{diag} \left(\frac{1}{R_1^2} \cdot \hat{\mathbf{A}}_1^{-1}, \frac{1}{R_2^2} \cdot \hat{\mathbf{A}}_2^{-1}, \dots, \frac{1}{R_N^2} \cdot \hat{\mathbf{A}}_N^{-1}, R_1^2 \cdot \hat{\mathbf{A}}_1, R_2^2 \cdot \hat{\mathbf{A}}_2, \dots, R_{N-1}^2 \cdot \hat{\mathbf{A}}_{N-1} \right) \quad (68)$$

is the core of our preconditioning strategy. The left multiplication of $\hat{\mathbf{Z}}$ by $\hat{\mathbf{Z}}$ and \mathbf{P} provides the same preconditioning effect presented in Section 4.1 for the single-layer operator case, capable of overcoming the dense-discretization breakdown of the symmetric formulation. The purpose of the introduction of the coefficients R_i in the formulation is to make the spectra of the matrices $\mathbf{Q}\hat{\mathbf{Z}}\mathbf{Q}$ and \mathbf{P} independent of the size of the geometry considered or, equivalently, independent of the unit of measure used for the definition of the mesh discretizing the head model.

Furthermore, we define the matrices

$$\mathbf{G} := \text{diag}(I_{N_{V,1},N_{V,1}}, I_{N_{V,2},N_{V,2}}, \dots, I_{N_{V,N},N_{V,N}} \mathbf{G}_{1,\lambda\pi}^{-1}, \mathbf{G}_{2,\lambda\pi}^{-1}, \dots, \mathbf{G}_{N-1,\lambda\pi}^{-1}) \quad (69)$$

and

$$\mathbf{M} := \text{diag}(\mathbf{G}_{1,\lambda\lambda}^{-1/2}, \mathbf{G}_{2,\lambda\lambda}^{-1/2}, \dots, \mathbf{G}_{N,\lambda\lambda}^{-1/2}, \mathbf{G}_{1,\pi\pi}^{-1/2}, \mathbf{G}_{2,\pi\pi}^{-1/2}, \dots, \mathbf{G}_{N-1,\pi\pi}^{-1/2}). \quad (70)$$

The left and right multiplication of the entire inner block $\mathbf{Q}\hat{\mathbf{Z}}\mathbf{Q}\mathbf{G}_L\mathbf{P}\mathbf{G}_R\mathbf{Q}\hat{\mathbf{Z}}\mathbf{Q}$ by \mathbf{M} results in a matrix spectrally equivalent to the one discretizing the continuous formulation with a set of orthonormal basis functions. One can be easily convinced of this by considering, for example, the simplifications leading to the equalities

$$\mathbf{G}_{1,\lambda\lambda}^{-1/2} \mathbf{N}_{11} \hat{\mathbf{A}}_1^{-1} \mathbf{N}_{11} \mathbf{G}_{1,\lambda\lambda}^{-1/2} = \left(\mathbf{G}_{1,\lambda\lambda}^{-1/2} \mathbf{N}_{11} \mathbf{G}_{1,\lambda\lambda}^{-1/2} \right) \left(\mathbf{G}_{1,\lambda\lambda}^{-1/2} \hat{\mathbf{A}}_1 \mathbf{G}_{1,\lambda\lambda}^{-1/2} \right)^{-1} \left(\mathbf{G}_{1,\lambda\lambda}^{-1/2} \mathbf{N}_{11} \mathbf{G}_{1,\lambda\lambda}^{-1/2} \right) \quad (71)$$

and

$$\begin{aligned} \mathbf{G}_{1,\pi\pi}^{-1/2} \mathbf{S}_{11} \mathbf{G}_{1,\lambda\pi}^{-1} \hat{\mathbf{A}}_1 \mathbf{G}_{1,\pi\lambda}^{-1} \mathbf{S}_{11} \mathbf{G}_{1,\pi\pi}^{-1/2} = \\ \left(\mathbf{G}_{1,\pi\pi}^{-1/2} \mathbf{S}_{11} \mathbf{G}_{1,\pi\pi}^{-1/2} \right) \left(\mathbf{G}_{1,\lambda\lambda}^{-1/2} \mathbf{G}_{1,\lambda\pi} \mathbf{G}_{1,\pi\lambda}^{-1/2} \right)^{-1} \left(\mathbf{G}_{1,\lambda\lambda}^{-1/2} \hat{\mathbf{A}}_1 \mathbf{G}_{1,\lambda\lambda}^{-1/2} \right) \left(\mathbf{G}_{1,\lambda\lambda}^{-1/2} \mathbf{G}_{1,\lambda\pi} \mathbf{G}_{1,\pi\lambda}^{-1/2} \right)^{-1} \left(\mathbf{G}_{1,\pi\pi}^{-1/2} \mathbf{S}_{11} \mathbf{G}_{1,\pi\pi}^{-1/2} \right) \end{aligned} \quad (72)$$

where the matrices

$$\left(\mathbf{G}_{1,\lambda\lambda}^{-1/2} \mathbf{N}_{11} \mathbf{G}_{1,\lambda\lambda}^{-1/2} \right), \quad \left(\mathbf{G}_{1,\pi\pi}^{-1/2} \mathbf{S}_{11} \mathbf{G}_{1,\pi\pi}^{-1/2} \right), \quad \left(\mathbf{G}_{1,\lambda\lambda}^{-1/2} \mathbf{G}_{1,\lambda\pi} \mathbf{G}_{1,\pi\lambda}^{-1/2} \right), \quad \left(\mathbf{G}_{1,\lambda\lambda}^{-1/2} \hat{\mathbf{A}}_1 \mathbf{G}_{1,\lambda\lambda}^{-1/2} \right), \quad \text{and} \quad \left(\mathbf{G}_{1,\lambda\lambda}^{-1/2} \hat{\mathbf{A}}_1 \mathbf{G}_{1,\lambda\lambda}^{-1/2} \right)$$

are spectrally equivalent to the discretizations of the hypersingular operator, the single-layer operator, the identity and the modified Laplace-Beltrami operator in orthonormal bases.

It is worth noticing at this moment that, although the direct evaluation of matrix \mathbf{M} could be expensive—indeed, it requires the square root decomposition of non-diagonal matrices, which can be expensive—it can easily be avoided. For example, by using a simple similarity transformation, we have [55]

$$\text{eig} \left(\mathbf{M}\mathbf{Q}\hat{\mathbf{Z}}\mathbf{Q}\mathbf{G}_L\mathbf{P}\mathbf{G}_R\mathbf{Q}\hat{\mathbf{Z}}\mathbf{Q}\mathbf{M} \right) = \text{eig} \left(\mathbf{M}\mathbf{M}\mathbf{Q}\hat{\mathbf{Z}}\mathbf{Q}\mathbf{G}\mathbf{P}\mathbf{G}^T\mathbf{Q}\hat{\mathbf{Z}}\mathbf{Q} \right), \quad (73)$$

where the symbol $\text{eig}(\mathbf{Z})$ denotes the set of eigenvalues of \mathbf{Z} . When the preconditioned conjugate gradient method [55] is employed to solve the system, the similarity transformation will not change the convergence behavior, thus, preserving the favorable convergence properties of the original system in (63).

Proposition 1. The coefficient matrix of the proposed formulation (63) is symmetric, positive-definite.

Proof. The matrix \mathbf{P} can be written as $\mathbf{P} = \mathbf{P}_{\text{sqrt}}^T \mathbf{P}_{\text{sqrt}}$ by virtue of its symmetric, positive-definiteness. Moreover, the matrices \mathbf{M} , \mathbf{Q} , \mathbf{Z} are symmetric and invertible. Therefore, we have the decomposition

$$\mathbf{M}\mathbf{Q}\hat{\mathbf{Z}}\mathbf{Q}\mathbf{G}\mathbf{P}\mathbf{G}^T\mathbf{Q}\hat{\mathbf{Z}}\mathbf{Q}\mathbf{M} = \left(\mathbf{P}_{\text{sqrt}} \mathbf{G}^T \mathbf{Q}\hat{\mathbf{Z}}\mathbf{Q}\mathbf{M} \right)^T \left(\mathbf{P}_{\text{sqrt}} \mathbf{G}^T \mathbf{Q}\hat{\mathbf{Z}}\mathbf{Q}\mathbf{M} \right) \quad (74)$$

ensuring the symmetric, positive-definiteness of the proposed formulation. \square

Before moving to the analysis of the conditioning properties of the new formulation, it is worth noting that the numerical scheme in (63) is refinement-free, that is, its implementation does not require the evaluation of integral operators on the dual mesh. Avoiding this operation sidesteps the computational burden of numerical integrations over the dual—and thus barycentrically refined mesh—leading to a significant advantage in terms of time required to build the formulation itself. In fact, in the proposed formulation (63) dual functions are only involved in the Gram matrices $(\mathbf{G}_{i,\tilde{\lambda}\pi})_{mn} = (\mathbf{G}_{i,\pi\tilde{\lambda}})_{nm} = \left(\tilde{\lambda}_{i,m}, \pi_{i,n}\right)_{L^2(\Gamma_i)}$ and in the Laplacian $(\tilde{\mathbf{D}}_i)_{mn} = \left(\nabla_{\Gamma_i} \tilde{\lambda}_{i,m} \nabla_{\Gamma_i} \tilde{\lambda}_{i,n}\right)_{L^2(\Gamma_i)}$, for which we have, unlike the system matrices stemming from integral operators, analytic expressions allowing a rapid evaluation (see [2]) and Appendix B for these expressions).

4.4. Proof of well-conditioning

In this section, we want to analyse the conditioning properties of the proposed formulation with respect to the two sources of instability identified in section 3, that are dense-discretization and high-contrast.

For proving the high-contrast stability, we note that $\text{cond}(\mathbf{Q}\hat{\mathbf{Z}}\mathbf{Q}) = O(1)$ for $CR := \max_i (CR_i) \rightarrow \infty$ directly follows from the discussion of the high-contrast spectral properties of $\mathbf{Q}\mathbf{Z}\mathbf{Q}$ in [42]. Then, we use the submultiplicativity of the condition number of matrix products

$$\text{cond}(\mathbf{Z}_p) \leq (\text{cond}(\mathbf{M}))^2 \left(\text{cond}(\mathbf{Q}\hat{\mathbf{Z}}\mathbf{Q})\right)^2 \text{cond}(\mathbf{G}\mathbf{P}\mathbf{G}^T), \quad (75)$$

which follows from the submultiplicativity of the Euclidean norms in the definition of condition number employed, that is $\text{cond}(\mathbf{Z}) = \|\mathbf{Z}\|_2 \|\mathbf{Z}^{-1}\|_2$ [47, Equation 2.1.25]. Next, we study the limit $\lim_{CR \rightarrow \infty}$

$$\lim_{CR \rightarrow \infty} \text{cond}(\mathbf{Z}_p) \leq \lim_{CR \rightarrow \infty} (\text{cond}(\mathbf{M}))^2 \left(\text{cond}(\mathbf{Q}\hat{\mathbf{Z}}\mathbf{Q})\right)^2 \text{cond}(\mathbf{G}\mathbf{P}\mathbf{G}^T). \quad (76)$$

Since the limits $\lim_{CR \rightarrow \infty} \text{cond}(\mathbf{M})$, $\lim_{CR \rightarrow \infty} \text{cond}(\mathbf{Q}\hat{\mathbf{Z}}\mathbf{Q})$, and $\lim_{CR \rightarrow \infty} \text{cond}(\mathbf{G}\mathbf{P}\mathbf{G}^T)$ are finite, the resulting limit (76), given by the product of them [50, Theorem 4.4], is finite, that is $\text{cond}(\mathbf{Z}_p) = O(1)$ as $CR \rightarrow \infty$, which concludes the proof of the high-contrast stability of our formulation.

For proving the dense-discretization stability of \mathbf{Z}_p , we will leverage a spectral analysis of the matrix in (63), first in the one-compartment case, then in the general N -compartment setup. The study is held on a spherical multi-compartment model, but, as before (Section 3), it can be extended to any geometry characterized by smooth boundaries without loss of generality.

4.4.1. One-compartment case

The matrix for which we are going to prove the dense-discretization stability reads

$$\begin{aligned} \mathbf{Z}_p = & \begin{pmatrix} \alpha_1 \mathbf{G}_{1,\lambda\lambda}^{-1/2} \hat{\mathbf{N}}_{11} \hat{\mathbf{D}}_1^{-1} \hat{\mathbf{N}}_{11} \mathbf{G}_{1,\lambda\lambda}^{-1/2} & \epsilon_1 \mathbf{G}_{1,\lambda\lambda}^{-1/2} \hat{\mathbf{N}}_{11} \hat{\mathbf{D}}_1^{-1} \mathbf{D}_{11}^* \mathbf{G}_{1,\pi\pi}^{-1/2} \\ \epsilon_1 \mathbf{G}_{1,\pi\pi}^{-1/2} \mathbf{D}_{11} \hat{\mathbf{D}}_1^{-1} \hat{\mathbf{N}}_{11} \mathbf{G}_{1,\lambda\lambda}^{-1/2} & \gamma_1 \mathbf{G}_{1,\pi\pi}^{-1/2} \mathbf{D}_{11} \hat{\mathbf{D}}_1^{-1} \mathbf{D}_{11}^* \mathbf{G}_{1,\pi\pi}^{-1/2} \end{pmatrix} \\ & + \begin{pmatrix} \beta_1 \mathbf{G}_{1,\lambda\lambda}^{-1/2} \mathbf{D}_{11}^* \mathbf{G}_{1,\lambda\pi}^{-1} \hat{\mathbf{D}}_1 \mathbf{G}_{1,\pi\lambda}^{-1} \mathbf{D}_{11} \mathbf{G}_{1,\lambda\lambda}^{-1/2} & \eta_1 \mathbf{G}_{1,\lambda\lambda}^{-1/2} \mathbf{D}_{11}^* \mathbf{G}_{1,\lambda\pi}^{-1} \hat{\mathbf{D}}_1 \mathbf{G}_{1,\pi\lambda}^{-1} \mathbf{S}_{11} \mathbf{G}_{1,\pi\pi}^{-1/2} \\ \eta_1 \mathbf{G}_{1,\pi\pi}^{-1/2} \mathbf{S}_{11} \mathbf{G}_{1,\lambda\pi}^{-1} \hat{\mathbf{D}}_1 \mathbf{G}_{1,\pi\lambda}^{-1} \mathbf{D}_{11} \mathbf{G}_{1,\lambda\lambda}^{-1/2} & \delta_1 \mathbf{G}_{1,\pi\pi}^{-1/2} \mathbf{S}_{11} \mathbf{G}_{1,\lambda\pi}^{-1} \hat{\mathbf{D}}_1 \mathbf{G}_{1,\pi\lambda}^{-1} \mathbf{S}_{11} \mathbf{G}_{1,\pi\pi}^{-1/2} \end{pmatrix} \end{aligned} \quad (77)$$

with the scalings

$$\begin{aligned} \alpha_1 &:= q_{V,1}^4 (\sigma_1 + \sigma_2)^2, & \beta_1 &:= 4R_1^2 (q_{V,1} q_{C,1})^2, \\ \epsilon_1 &:= -\frac{2}{R_1} q_{V,1}^2 (q_{V,1} q_{C,1}) (\sigma_1 + \sigma_2), & \delta_1 &:= q_{C,1}^4 (\sigma_1^{-1} + \sigma_2^{-1})^2, \\ \gamma_1 &:= \frac{4}{R_1^2} (q_{V,1} q_{C,1})^2, & \eta_1 &:= -2R_1 q_{C,1}^2 (q_{V,1} q_{C,1}) (\sigma_1^{-1} + \sigma_2^{-1}) \dots \end{aligned}$$

For the reasons presented in Section 4.1, the matrix $\mathbf{G}_{1,\pi\pi}^{-1/2} \mathbf{S}_{11} \hat{\mathbf{D}}_{\pi,1} \mathbf{S}_{11} \mathbf{G}_{1,\pi\pi}^{-1/2}$, discretizing the second kind operator $\mathbf{S}_{11} \hat{\Delta}_{\Gamma_1} \mathbf{S}_{11} = \frac{\Gamma}{4} + \mathcal{K}_{\mathbf{S}_{11} \hat{\Delta}_{\Gamma_1} \mathbf{S}_{11}}$, is well-conditioned and its spectrum accumulates at $1/4$. An accurate study is needed to understand the nature of all the other blocks.

Proposition 2. The matrix $\mathbf{G}_{1,\lambda\lambda}^{-1/2} \hat{\mathbf{N}}_{11} \hat{\mathbf{A}}_1^{-1} \hat{\mathbf{N}}_{11} \mathbf{G}_{1,\lambda\lambda}^{-1/2}$ is well-conditioned and its spectrum accumulates at $1/4$.

Proof. From the Calderón relations, by expanding the products $\mathcal{S}\hat{\mathcal{N}}$ and $\hat{\mathcal{N}}\mathcal{S}$, we obtain that

$$-\mathcal{S}\hat{\mathcal{N}} = \frac{\mathcal{I}}{4} + \mathcal{K}_{\mathcal{S}\hat{\mathcal{N}}} \quad (78)$$

$$-\hat{\mathcal{N}}\mathcal{S} = \frac{\mathcal{I}}{4} + \mathcal{K}_{\hat{\mathcal{N}}\mathcal{S}}, \quad (79)$$

where $\mathcal{K}_{\mathcal{S}\hat{\mathcal{N}}}, \mathcal{K}_{\hat{\mathcal{N}}\mathcal{S}}$ are compact operators. By exploiting these relations for simplifying the product $\mathcal{S}\hat{\Delta}_r \mathcal{S}\hat{\mathcal{N}}\hat{\Delta}_r^{-1}\hat{\mathcal{N}}$, it is found that $\hat{\mathcal{N}}\hat{\Delta}_r^{-1}\hat{\mathcal{N}}$ is a second kind operator with accumulation point at $1/4$. Indeed

$$\begin{aligned} \mathcal{S}\hat{\Delta}_r \mathcal{S}\hat{\mathcal{N}}\hat{\Delta}_r^{-1}\hat{\mathcal{N}} &= -\mathcal{S}\hat{\Delta}_r \left(\frac{\mathcal{I}}{4} + \mathcal{K}_{\mathcal{S}\hat{\mathcal{N}}} \right) \hat{\Delta}_r^{-1}\hat{\mathcal{N}} \\ &= -\frac{1}{4}\mathcal{S}\hat{\mathcal{N}} - \mathcal{S}\hat{\Delta}_r \mathcal{K}_{\mathcal{S}\hat{\mathcal{N}}}\hat{\Delta}_r^{-1}\hat{\mathcal{N}} \\ &= \frac{\mathcal{I}}{16} + \frac{1}{4}\mathcal{K}_{\mathcal{S}\hat{\mathcal{N}}} - \mathcal{S}\hat{\Delta}_r \mathcal{K}_{\mathcal{S}\hat{\mathcal{N}}}\hat{\Delta}_r^{-1}\hat{\mathcal{N}}, \end{aligned} \quad (80)$$

where $\mathcal{S}\hat{\Delta}_r \mathcal{K}_{\mathcal{S}\hat{\mathcal{N}}}\hat{\Delta}_r^{-1}\hat{\mathcal{N}}$ is compact as the product of compact and of bounded linear operators is compact [16, Theorem 1.5]. Therefore, equation (80) implies $\hat{\mathcal{N}}\hat{\Delta}_r^{-1}\hat{\mathcal{N}} = \mathcal{I}/4 + \mathcal{K}_{\hat{\mathcal{N}}\hat{\Delta}_r^{-1}\hat{\mathcal{N}}}$. The discretization of this second-kind operator with an orthonormal set of basis functions, as in $\mathbf{G}_{1,\lambda\lambda}^{-1/2} \hat{\mathbf{N}}_{11} \hat{\mathbf{A}}_1^{-1} \hat{\mathbf{N}}_{11} \mathbf{G}_{1,\lambda\lambda}^{-1/2}$, results thus in a well-conditioned matrix with its eigenvalues accumulating at $1/4$. \square

From a spherical harmonic analysis held on a sphere of radius R_1 , we recognize that the eigenvalues of the operator $\mathcal{D}^* \Delta_r \mathcal{D}$ are the product of the eigenvalues of \mathcal{D}^* , Δ_r , and \mathcal{D} ,

$$\frac{1}{R_1^2} \frac{1}{2(2n+1)} n(n+1) \frac{1}{2(2n+1)} = \frac{1}{R_1^2} \frac{n^2+n}{16n^2+16n+4}, \quad (81)$$

since the operators \mathcal{D}^* , Δ_r , and \mathcal{D} have the same eigenvectors [31, 18]. Therefore, by analyzing the limit of (81) for $n \rightarrow \infty$, it is possible to state that $\mathcal{D}^* \Delta_r \mathcal{D}$ is a second-kind operator with accumulation point $1/(16R_1^2)$. Hence, since the modified operator $\hat{\Delta}_r$ provides similar spectral properties to Δ_r , the discretized form $R_1^2 \mathbf{G}_{1,\lambda\lambda}^{-1/2} \mathcal{D}^*_{11} \mathbf{G}_{1,\lambda\pi}^{-1} \hat{\mathbf{A}}_1 \mathbf{G}_{1,\pi\lambda}^{-1} \mathcal{D}_{11} \mathbf{G}_{1,\lambda\lambda}^{-1/2}$ on spherical geometries is well-conditioned and its spectrum accumulates at $1/16$.

Similarly, the expression of the eigenvalues of the two operators $\mathcal{D}^* \Delta_r \mathcal{S}$ and $\mathcal{S} \Delta_r \mathcal{D}$ is given by

$$-\frac{1}{R_1} \frac{1}{2(2n+1)} n(n+1) \frac{1}{2n+1} = -\frac{1}{R_1} \frac{n^2+n}{8n^2+8n+2}, \quad (82)$$

from which we deduce that $\mathcal{D}^* \Delta_r \mathcal{S}$ and $\mathcal{S} \Delta_r \mathcal{D}$ are second-kind operators with eigenvalues accumulating at $-1/(8R_1)$ and the matrices $R_1 \mathbf{G}_{1,\lambda\lambda}^{-1/2} \mathcal{D}^*_{11} \mathbf{G}_{1,\lambda\pi}^{-1} \hat{\mathbf{A}}_1 \mathbf{G}_{1,\pi\lambda}^{-1} \mathcal{S}_{11} \mathbf{G}_{1,\pi\pi}^{-1/2}$ and $R_1 \mathbf{G}_{1,\pi\pi}^{-1/2} \mathcal{S}_{11} \mathbf{G}_{1,\lambda\pi}^{-1} \hat{\mathbf{A}}_1 \mathbf{G}_{1,\pi\lambda}^{-1} \mathcal{D}_{11} \mathbf{G}_{1,\lambda\lambda}^{-1/2}$ discretizing the operators on a sphere are well-conditioned with spectra accumulating at $1/8$. Since a smooth variation from a spherical geometry only results in a compact perturbation [34, 56], the results mentioned above hold true also for non-spherical, smooth geometries, such as the ones considered in this work.

Proposition 3. The matrices $\mathbf{G}_{1,\lambda\lambda}^{-1/2} \hat{\mathbf{N}}_{11} \hat{\mathbf{A}}_1^{-1} \mathcal{D}^*_{11} \mathbf{G}_{1,\pi\pi}^{-1/2}$, $\mathbf{G}_{1,\pi\pi}^{-1/2} \mathcal{D}_{11} \hat{\mathbf{A}}_1^{-1} \hat{\mathbf{N}}_{11} \mathbf{G}_{1,\lambda\lambda}^{-1/2}$, and $\mathbf{G}_{1,\pi\pi}^{-1/2} \mathcal{D}_{11} \hat{\mathbf{A}}_1^{-1} \mathcal{D}^*_{11} \mathbf{G}_{1,\pi\pi}^{-1/2}$ discretize compact operators, that is, their spectra accumulate at 0.

Proof. The operators $\hat{\mathcal{N}}\hat{\Delta}_r^{-1}\mathcal{D}^*$, $\mathcal{D}\hat{\Delta}_r^{-1}\hat{\mathcal{N}}$, and $\mathcal{D}\hat{\Delta}_r^{-1}\mathcal{D}^*$ are compact, as they can be written as the product of second kind and compact operators [16, Theorem 1.5], as

$$\begin{aligned} \hat{\mathcal{N}}\hat{\Delta}_r^{-1}\mathcal{D}^* &= \hat{\mathcal{N}}\hat{\Delta}_r^{-1}\hat{\mathcal{N}}\hat{\mathcal{N}}^{-1}\mathcal{D}^*, \\ \mathcal{D}\hat{\Delta}_r^{-1}\hat{\mathcal{N}} &= \mathcal{D}\hat{\mathcal{N}}^{-1}\hat{\mathcal{N}}\hat{\Delta}_r^{-1}\hat{\mathcal{N}}, \\ \mathcal{D}\hat{\Delta}_r^{-1}\mathcal{D}^* &= \mathcal{D}\hat{\mathcal{N}}^{-1}\hat{\mathcal{N}}\hat{\Delta}_r^{-1}\hat{\mathcal{N}}\hat{\mathcal{N}}^{-1}\mathcal{D}^*, \end{aligned}$$

where $\hat{\mathcal{N}}^{-1}\mathcal{D}^*$ and $\mathcal{D}\hat{\mathcal{N}}^{-1}$ are compact operators, composed out of bounded operators, where at least one is compact [16, Theorem 1.5]. Therefore, their discretization results in ill-conditioned matrices with vanishing spectra. \square

Given the considerations above, matrix (77) can be written as

$$\begin{pmatrix} (\alpha_1 + \beta_1/4)/4 I_{N_{V,1},N_{V,1}} & \eta_1/8 I_{N_{V,1},N_{C,1}} \\ \eta_1/8 I_{N_{C,1},N_{V,1}} & \delta_1/4 I_{N_{C,1},N_{C,1}} \end{pmatrix} + \begin{pmatrix} \mathbf{K}_{N_{V,1},N_{V,1}} & \mathbf{K}_{N_{V,1},N_{C,1}} \\ \mathbf{K}_{N_{C,1},N_{V,1}} & \mathbf{K}_{N_{C,1},N_{C,1}} \end{pmatrix}, \quad (83)$$

where $\mathbf{K}_{m,n} \in \mathbb{R}^{m \times n}$ represents the discretization of a compact operator. As is clear from their expression, α_1 and β_1 are positive scalar coefficients, so that the principal part of the top-left block of (77) cannot be canceled. The second term in the summation (83) is the discretization of a block operator with compact blocks, and thus is compact (proof in Appendix A), with singular values accumulating at zero when increasing the number of degrees of freedom of the system, and as a consequence it does not influence the spectral properties of the system asymptotically. Therefore, in order to analyze the boundness of the condition number of the system away from singularities, it is sufficient to study the spectral behaviour of the principal part in (83). This can be established by the analytical evaluation of the eigenvalues of the principal term in (83), performed by means of a Schur analysis [61]. In particular, in the case $N_{C,1} \geq N_{V,1}$ it is found that

$$\lambda_1 = \frac{\delta_1}{4}, \quad \text{with multiplicity } N_{C,1} - N_{V,1} \quad (84)$$

$$\lambda_2 = \frac{1}{32} \left(4\alpha_1 + \beta_1 + 4\delta_1 - \sqrt{(4\alpha_1 + \beta_1 - 4\delta_1)^2 + 16\eta_1^2} \right), \quad \text{with multiplicity } N_{V,1} \quad (85)$$

$$\lambda_3 = \frac{1}{32} \left(4\alpha_1 + \beta_1 + 4\delta_1 + \sqrt{(4\alpha_1 + \beta_1 - 4\delta_1)^2 + 16\eta_1^2} \right), \quad \text{with multiplicity } N_{V,1}; \quad (86)$$

in the case $N_{C,1} < N_{V,1}$ instead, the eigenvalues are

$$\lambda_1 = \frac{4\alpha_1 + \beta_1}{16}, \quad \text{with multiplicity } N_{V,1} - N_{C,1} \quad (87)$$

$$\lambda_2 = \frac{1}{32} \left(4\alpha_1 + \beta_1 + 4\delta_1 - \sqrt{(4\alpha_1 + \beta_1 - 4\delta_1)^2 + 16\eta_1^2} \right), \quad \text{with multiplicity } N_{C,1} \quad (88)$$

$$\lambda_3 = \frac{1}{32} \left(4\alpha_1 + \beta_1 + 4\delta_1 + \sqrt{(4\alpha_1 + \beta_1 - 4\delta_1)^2 + 16\eta_1^2} \right), \quad \text{with multiplicity } N_{C,1}. \quad (89)$$

Hence, the condition number of the principal part of \mathbf{Z} , that is symmetric, positive-definite, is given by

$$\max(\lambda_1, \lambda_2, \lambda_3) / \min(\lambda_1, \lambda_2, \lambda_3),$$

independent of mesh refinement. Therefore, the condition number of the overall matrix \mathbf{Z} when asymptotically increasing the number of degrees of freedom of the system is bounded and the proposed system is well-conditioned with respect to dense discretizations.

Moreover, given the asymptotic behaviours

$$\begin{aligned} \alpha_1 &= \mathcal{O}(1), & \beta_1 &= \mathcal{O}(CR_1^{-1}), \\ |\epsilon_1| &= \mathcal{O}(CR_1^{-1/2}), & \delta_1 &= \mathcal{O}(1), \\ \gamma_1 &= \mathcal{O}(CR_1^{-1}), & |\eta_1| &= \mathcal{O}(CR_1^{-1/2}). \end{aligned}$$

valid in the limit $CR_1 \rightarrow \infty$, we observe that the condition number of the principal part of \mathbf{Z} tends to unity in the high-contrast regime, as α_1 approaches δ_1 , that is $(\max(\lambda_1, \lambda_2, \lambda_3) / \min(\lambda_1, \lambda_2, \lambda_3)) - 1 = \mathcal{O}(CR_1^{-1/2})$ for $CR_1 \rightarrow \infty$.

4.4.2. N -compartment case

For the generic, N -layered geometry, the matrix \mathbf{Z}_p in (63) can be written as

$$\left(\begin{array}{cccc} (\alpha_1 + \beta_1/4)/4 \mathbf{I}_{N_V,1,N_V,1} & & \eta_1/8 \mathbf{I}_{N_V,1,N_C,1} & \\ & \ddots & & \ddots \\ \eta_1/8 \mathbf{I}_{N_C,1,N_V,1} & & (\alpha_N + \beta_N/4)/4 \mathbf{I}_{N_V,N,N_V,N} & \eta_N/8 \mathbf{I}_{N_V,N,N_C,N} \\ & & \delta_1/4 \mathbf{I}_{N_C,1,N_C,1} & \\ & & & \ddots \\ & & \eta_N/8 \mathbf{I}_{N_C,N,N_V,N} & \delta_N/4 \mathbf{I}_{N_C,N,N_C,N} \end{array} \right) + \mathbf{K} \quad (90)$$

where the scaling coefficients are

$$\begin{aligned} \alpha_n &:= q_{V,n}^4 (\sigma_n + \sigma_{n+1})^2, & \delta_n &:= q_{C,n}^4 (\sigma_n^{-1} + \sigma_{n+1}^{-1})^2, \\ \beta_n &:= 4R_n^2 (q_{V,n} q_{C,n})^2, & \eta_n &:= -2R_n q_{C,n}^2 (q_{V,n} q_{C,n}) (\sigma_n^{-1} + \sigma_{n+1}^{-1}), \end{aligned}$$

with subscript $n = 1, \dots, N$. The matrix \mathbf{K} is a $(2N \times 2N)$ -block matrix, discretizing a compact, block operator (see Appendix A). Indeed, each block of \mathbf{K} is a linear combination of matrices discretizing compact operators, either in the form,

$$\hat{\mathcal{N}}_{ij} \hat{\Delta}_{\Gamma_j}^{-1} \mathcal{D}_{jk}^*, \quad \mathcal{D}_{ij} \hat{\Delta}_{\Gamma_j}^{-1} \hat{\mathcal{N}}_{jk}, \quad \mathcal{D}_{ij} \hat{\Delta}_{\Gamma_j}^{-1} \mathcal{D}_{jk}^*, \quad (91)$$

whose compactness has already been discussed in the proof of Proposition 3, or in the form

$$\hat{\mathcal{N}}_{ij} \hat{\Delta}_{\Gamma_j}^{-1} \hat{\mathcal{N}}_{jk}, \quad \mathcal{S}_{ij} \hat{\Delta}_{\Gamma_j} \mathcal{S}_{jk}, \quad \mathcal{D}_{ij}^* \hat{\Delta}_{\Gamma_j} \mathcal{D}_{jk}, \quad \mathcal{D}_{ij}^* \hat{\Delta}_{\Gamma_j} \mathcal{S}_{jk}, \quad \mathcal{S}_{ij} \hat{\Delta}_{\Gamma_j} \mathcal{D}_{jk}, \quad (92)$$

with $i \neq j$ or $j \neq k$, resulting from the product of bounded and compact operators [16, Theorem 1.5].

As in the one-compartment case, the analytic spectral analysis of the principal part of (90), when fixing the number of compartments N , is useful to determine the asymptotic spectral behaviour of the overall matrix \mathbf{Z}_p when increasing the number of unknowns. In the general case, we can argue that, since the coefficients α_n , β_n , δ_n , and η_n are independent from the refinement parameter h , also the condition number of the principal part of (90) is h -independent.

In addition, we can perform an asymptotic analysis of the principal part of (90) for the contrast ratio going to infinity, providing some insights in the spectral behaviour of the proposed formulation in the high-contrast and dense-discretization limit. We can assume, for example, an N -compartment structure (with N odd) with conductivities $\sigma_{1+2n} = \sigma_{\text{high}}$ and $\sigma_{2+2n} = \sigma_{\text{low}}$, for n running from 0 to $(N-1)/2$, satisfying $CR = \sigma_{\text{high}}/\sigma_{\text{low}} \rightarrow \infty$. Then, the behaviour of the scalar scalings is

$$\begin{aligned} \alpha_i &= \mathcal{O}(1), & \beta_i &= \mathcal{O}(CR^{-1}), \\ |\eta_i| &= \mathcal{O}(CR^{-1/2}), & \delta_i &= \mathcal{O}(1), \end{aligned}$$

resulting in the behaviour of the condition number of the principal part of \mathbf{Z}_p as $(\text{cond}(\mathbf{Z}_p - \mathbf{K}) - 1) = \mathcal{O}(CR^{-1/2})$ as $CR \rightarrow \infty$.

The asymptotic form above highlights the fact that the designed preconditioning is optimized for high-contrast structures. Nevertheless, the proposed formulation remains stable in the whole range of conductivity ratios commonly employed to model the head biological tissues, as shown in the numerical results Section 5.

5. Numerical results

The numerical results reported in this section showcase the efficacy of the proposed formulation and offer a comparison with the standard symmetric formulation. To this end, we first apply the numerical schemes to the canonical, spherical, head model, for which the analytic solution is available as a benchmark [20, 65]. Then, we move on to a more realistic head model, extracted from magnetic resonance imaging data, over which we solve the inverse EEG problem.

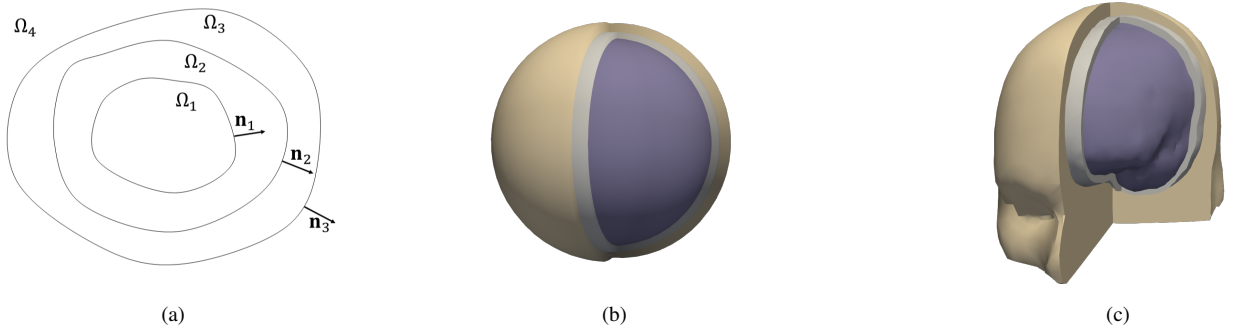


Fig. 3. (a) Schematic representation of the geometry under study. (b) The spherical and (c) the realistic, MRI-obtained head models. The three-compartments represent the brain, the skull and the skin.

5.1. The spherical head model

A three-compartment head model is considered in this section, delimited by the spherical surfaces Γ_1 , Γ_2 , and Γ_3 with radii $R_1 = 8.7$ cm, $R_2 = 9.2$ cm, and $R_3 = 10$ cm. In this first set of experiments, the source employed is a single dipole, placed inside Ω_1 at a distance of 4.2 cm from Γ_1 and radially directed. The conductivities of the three layers, modelling the brain, the skull and the scalp, have been set to $\sigma_1 = \frac{1}{3}$ S/m, $\sigma_2 = \frac{1}{240}$ S/m, and $\sigma_3 = \frac{1}{3}$ S/m, as typical in these models.

As first assessment, we verify the convergence rate of our new formulation, similar as in the unpreconditioned symmetric formulation case with same accuracy levels as shown in Figure 4.

Next we assess the efficacy of our preconditioner. In Figure 5, the variation of the condition number as a function of the inverse refinement parameter $1/h$ is reported for the two formulations considered. The efficacy of the preconditioning strategy is demonstrated by the constant conditioning in refinement, while the condition number of the symmetric formulation grows with the discretization as $\mathcal{O}(h^{-2})$. A similar behaviour is reflected in Figure 6a, where the number of iterations to solve the system up to a fixed level of accuracy is reported for the two formulations. The iterative method employed to solve the system in the two cases is the conjugate gradient-squared (CGS) solver [57].

The linear system arising from the preconditioning scheme presented in this work can also be solved by means of a preconditioned conjugate gradient (PCG) scheme [30, 58], by virtue of its symmetric, positive, definiteness properties. The preconditioning matrix is M^2 , as explained in Section 4.3. The number of matrix-vector products required for the solution, corresponding to the number of iterations, is shown in Figure 6b in green. This can be compared with the number of matrix-vector products (two per iteration) required to solve the symmetric formulation and the proposed preconditioned formulation by means of the conjugate gradient squared solver, at the same level of accuracy, shown in the same figure.

The efficacy of the proposed preconditioning has to be tested also for different values of conductivity contrasts between adjacent compartments. Experimental evidences from in vivo measurements have shown that the conductivity ratio between brain, skull, and scalp range between (1:1/15:1) and (1:1/80:1) [25, 64, 15]. So, we evaluated the stability of our formulation for conductivity ratios spanning from (1:1/10:1) to (1:1/100:1). Figure 7a, showing the number of iterations of the CGS solver as a function of the conductivity contrast ratio, gives evidence of the preconditioning effect obtained. The number of matrix-vector products required to solve the proposed formulation by means of the conjugate gradient scheme is also shown in Figure 7b and compared with the one required for solving both the symmetric formulation and the proposed scheme by means of the CGS solver.

5.2. The MRI-obtained head model

Subsequently, a realistic three-compartment head model obtained from MRI data has been considered. The boundaries of the geometry have been discretized by means of the meshes Γ_1 , with $N_{C,1} = 3684$, $N_{V,1} = 1844$, Γ_2 , with $N_{C,2} = 2334$, $N_{V,2} = 1169$, and Γ_3 , with $N_{C,3} = 2086$, $N_{V,3} = 1045$. The conductivities of the tissues have been set at $\sigma_1 = \frac{1}{3}$ S/m, $\sigma_2 = \frac{1}{150}$ S/m, and $\sigma_3 = \frac{1}{3}$ S/m. The neural source has been modelled by a point dipole placed inside the inner compartment at a distance of approximately 3.5 cm from Γ_1 . Figure 8a shows the resulting potential distribution on the exterior layer. Moreover, the absolute difference of this result with respect to the one obtained from

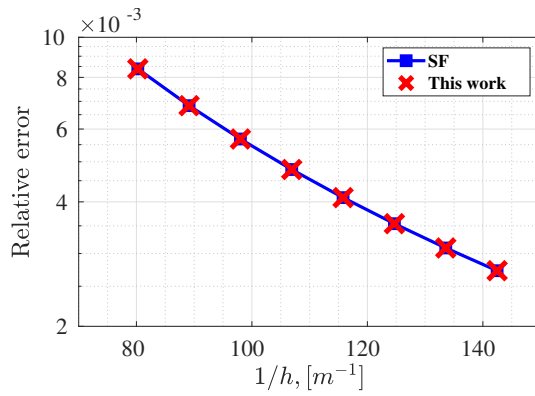


Fig. 4. Relative error between the numerical solution and the analytic solution for the potential on T_3 against the inverse mesh refinement parameter $1/h$: comparison between the symmetric formulation (SF) and this work.

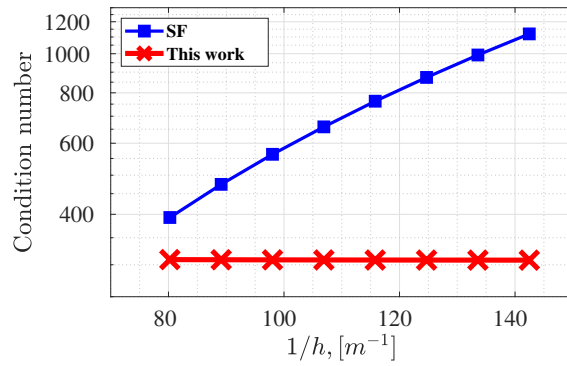


Fig. 5. Condition number as a function of the inverse mesh refinement parameter $1/h$: comparison between the symmetric formulation (SF) and this work.

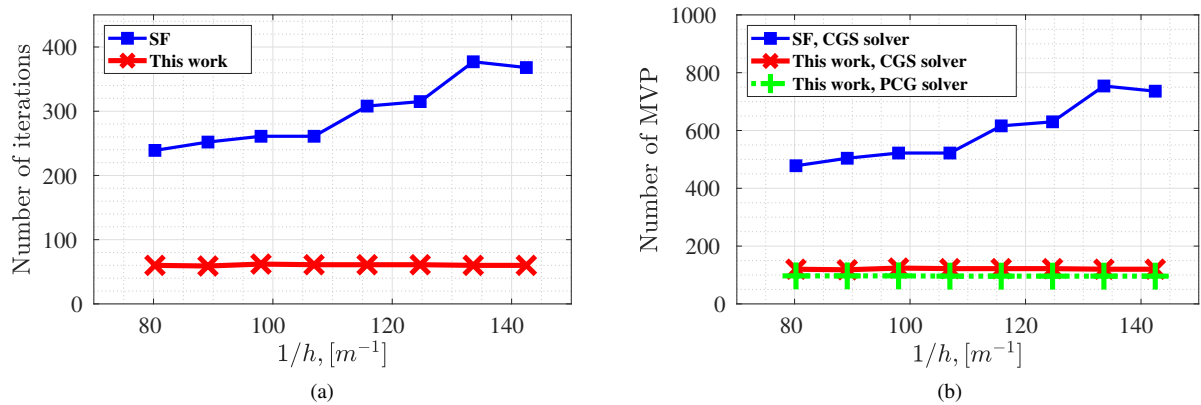


Fig. 6. (a) Number of iterations and (b) number of matrix-vector products (MVP) as a function of the inverse mesh refinement parameter $1/h$: comparison between the symmetric formulation (SF) and this work.

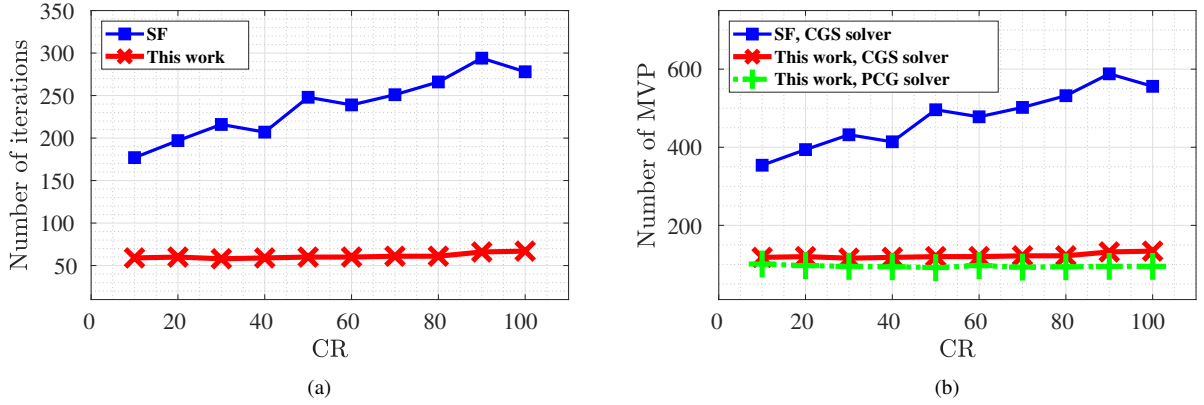


Fig. 7. (a) Number of iterations and (b) number of matrix-vector products (MVP) as a function of the conductivity ratio CR : comparison between the symmetric formulation (SF) and this work at $1/h \approx 80.2 \text{ m}^{-1}$.

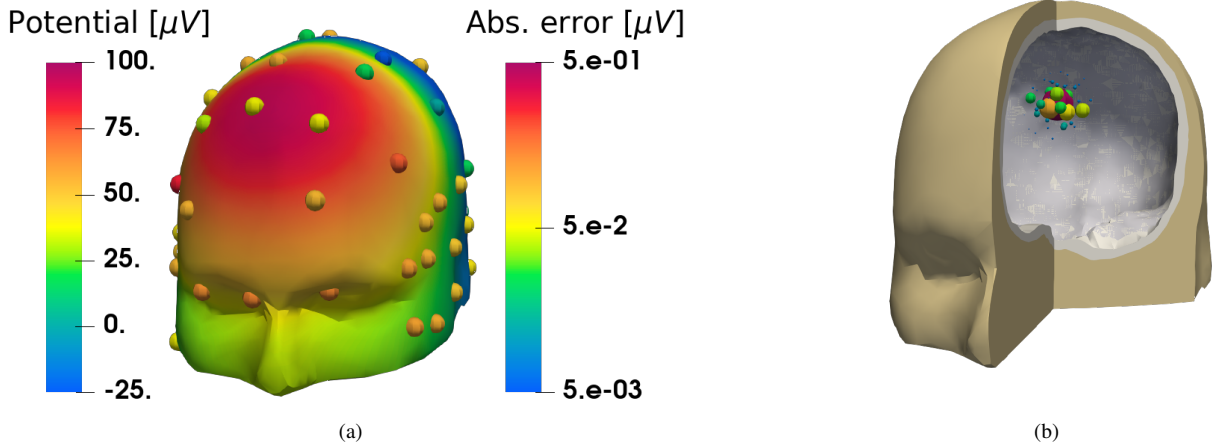


Fig. 8. (a) Scalp potential distribution and error at the electrodes with respect to the symmetric formulation solution. (b) Reconstructed epileptogenic source.

the unpreconditioned symmetric formulation is reported in correspondence of the position of 65 electrodes placed on the scalp. The linear system of 10 076 equations arising from the proposed formulation has been solved iteratively by means of the CGS solver in 155 iterations, to be compared with the 2157 iterations needed to solve the symmetric formulation by means of the same solver and by imposing an identical tolerance.

Given the excellent agreement in the results from the two formulations, the proposed scheme can clearly be employed in the evaluation of the lead-field matrix needed for the solution of the inverse EEG problem, at a reduced computational cost compared with the non-preconditioned one. The outcome of this test is shown in Figure 8b, where the neural source reconstructed from EEG measurements is represented. In particular, this has been obtained by applying the sLORETA inversion algorithm [43] to a lead-field matrix $\mathbf{G} \in \mathbb{R}^{N_E \times N_D}$, where $N_E = 65$ is the number of measurement points (corresponding to the number of electrodes) and $N_D = 19279$ is the number of test dipoles uniformly placed inside Ω_1 .

Appendix A. Proof of compactness of a block operator with compact blocks

This section will provide a proof for the compactness of a 2×2 block operator with compact blocks, that is, whose blocks are compact operators, rearranged from [44]. As a corollary, the compactness of a $N \times N$ block operator with

compact blocks is shown.

Given the normed spaces X_1, X_2, \dots, X_N , their Cartesian product, denoted as $X_1 \oplus X_2 \dots \oplus X_N$, equipped with the norm

$$\|(x_1, x_2, \dots, x_N)\|_{\oplus_{i=1}^N X_i} := \left(\sum_{i=1}^N \|x_i\|_{X_i}^2 \right)^{1/2}, \quad (\text{A.1})$$

is their direct sum normed space [1], needed in the following derivations.

Proposition 4. Given the compact operators $\mathcal{K}_{11} : X \rightarrow X$ and $\mathcal{K}_{22} : Y \rightarrow Y$, the block operator

$$\mathcal{K}_d := \begin{pmatrix} \mathcal{K}_{11} & 0 \\ 0 & \mathcal{K}_{22} \end{pmatrix} : X \oplus Y \rightarrow X \oplus Y \quad (\text{A.2})$$

is compact.

Proof. Let $\{u_n\} = \{(x_n, y_n)\}$ be a bounded sequence in $X \oplus Y$, that is, there exists a real positive constant c such that

$$\|u_n\|_{X \oplus Y}^2 = \|x_n\|_X^2 + \|y_n\|_Y^2 \leq c. \quad (\text{A.3})$$

This implies that $\{x_n\}$ and $\{y_n\}$ are bounded in X and in Y . Therefore, by virtue of the compactness of \mathcal{K}_{11} , the sequence $\{\mathcal{K}_{11}x_n\}$ contains a convergent subsequence [16, Theorem 1.2], denoted by $\{\mathcal{K}_{11}x_{n_{i_k}}\}$. Due to the boundness of $\{y_n\}$, also $\{y_{n_i}\}$ is bounded. Hence, $\{\mathcal{K}_{22}y_{n_i}\}$ contains a convergent subsequence, denoted as $\{\mathcal{K}_{22}y_{n_{i_k}}\}$. Clearly, also $\{\mathcal{K}_{11}x_{n_{i_k}}\}$ is convergent, as subsequence of a convergent subsequence.

In symbols, $\forall \epsilon > 0, \exists K$ such that $\forall k > K$

$$\|\mathcal{K}_{11}x_{n_{i_k}} - l_x\|_X < \epsilon \quad \text{and} \quad \|\mathcal{K}_{22}y_{n_{i_k}} - l_y\|_Y < \epsilon. \quad (\text{A.4})$$

It follows that the application of the operator \mathcal{K}_d to the bounded sequence $\{u_n\}$, reading

$$\{\mathcal{K}_d u_n\} = \{(\mathcal{K}_{11}x_n, \mathcal{K}_{22}y_n)\} \quad (\text{A.5})$$

contains the convergent subsequence $\{\mathcal{K}_d u_{n_{i_k}}\} = \{(\mathcal{K}_{11}x_{n_{i_k}}, \mathcal{K}_{22}y_{n_{i_k}})\}$. Indeed, $\forall k > K$

$$\|\mathcal{K}_d u_{n_{i_k}} - \begin{pmatrix} l_x \\ l_y \end{pmatrix}\|_{X \oplus Y} = \left(\|\mathcal{K}_{11}x_{n_{i_k}} - l_x\|_X^2 + \|\mathcal{K}_{22}y_{n_{i_k}} - l_y\|_Y^2 \right)^{1/2} \leq \sqrt{2}\epsilon = \epsilon', \quad (\text{A.6})$$

which concludes the proof. □

Proposition 5. Given the compact operators $\mathcal{K}_{12} : Y \rightarrow X$ and $\mathcal{K}_{21} : X \rightarrow Y$, the block operator

$$\mathcal{K}_{od} := \begin{pmatrix} 0 & \mathcal{K}_{12} \\ \mathcal{K}_{21} & 0 \end{pmatrix} : X \oplus Y \rightarrow X \oplus Y \quad (\text{A.7})$$

is compact.

Proof. We follow similar steps as in the proof of Proposition 4. Let $\{u_n\}$ be a bounded sequence as above. Given the compactness of \mathcal{K}_{12} , the sequence $\{\mathcal{K}_{12}y_n\}$ contains a converging subsequence, denoted by $\{\mathcal{K}_{12}y_{n_i}\}$. Then, we notice that the compact operator \mathcal{K}_{21} applied to the bounded subsequence x_{n_i} contains a converging subsequence, noted as $x_{n_{i_k}}$. Finally, $\forall \epsilon > 0, \exists K'$ such that $\forall k > K'$

$$\|\mathcal{K}_{12}y_{n_{i_k}} - l'_x\|_X < \epsilon \quad \text{and} \quad \|\mathcal{K}_{21}x_{n_{i_k}} - l'_y\|_Y < \epsilon. \quad (\text{A.8})$$

Therefore, the sequence $\{\mathcal{K}_{od}u_n\}$ contains a converging subsequence, denoted by $\{\mathcal{K}_{od}u_{n_{i_k}}\}$. Indeed, $\forall k > K'$,

$$\|\mathcal{K}_{od}u_{n_{i_k}} - \begin{pmatrix} l'_x \\ l'_y \end{pmatrix}\|_{X \oplus Y} = \left(\|\mathcal{K}_{12}y_{n_{i_k}} - l'_x\|_X^2 + \|\mathcal{K}_{21}x_{n_{i_k}} - l'_y\|_Y^2 \right)^{1/2} \leq \sqrt{2}\epsilon = \epsilon', \quad (\text{A.9})$$

hence \mathcal{K}_{od} is compact. □

Theorem 1. Given the compact operators $\mathcal{K}_{11} : X \rightarrow X$, $\mathcal{K}_{12} : Y \rightarrow X$, $\mathcal{K}_{21} : X \rightarrow Y$, and $\mathcal{K}_{22} : Y \rightarrow Y$, the block operator

$$\mathcal{K} = \begin{pmatrix} \mathcal{K}_{11} & \mathcal{K}_{12} \\ \mathcal{K}_{21} & \mathcal{K}_{22} \end{pmatrix} : X \oplus Y \rightarrow X \oplus Y \quad (\text{A.10})$$

is compact.

Proof. The operator \mathcal{K} can be written as the sum of two operators involving the diagonal and the off-diagonal terms, named respectively \mathcal{K}_d and \mathcal{K}_{od} ,

$$\mathcal{K} = \underbrace{\begin{pmatrix} \mathcal{K}_{11} & 0 \\ 0 & \mathcal{K}_{22} \end{pmatrix}}_{\mathcal{K}_d} + \underbrace{\begin{pmatrix} 0 & \mathcal{K}_{12} \\ \mathcal{K}_{21} & 0 \end{pmatrix}}_{\mathcal{K}_{od}}. \quad (\text{A.11})$$

The two operators \mathcal{K}_d and \mathcal{K}_{od} are compact, as shown in Proposition 4 and Proposition 5. Therefore, \mathcal{K} is compact as the sum of compact operators [16, Theorem 1.4]. \square

Corollary 1. Any block operator whose blocks are compact operators is compact.

Proof. A $N \times N$ block operator whose blocks are compact can be decomposed as the summation of $(2N - 1)$ block operators, each of them null apart one diagonal (principal or not), equal to the same diagonal of the original operator. For example, in the case $N = 3$,

$$\begin{aligned} \mathcal{K} &= \begin{pmatrix} \mathcal{K}_{11} & \mathcal{K}_{12} & \mathcal{K}_{13} \\ \mathcal{K}_{21} & \mathcal{K}_{22} & \mathcal{K}_{23} \\ \mathcal{K}_{31} & \mathcal{K}_{32} & \mathcal{K}_{33} \end{pmatrix} \\ &= \begin{pmatrix} 0 & 0 & 0 \\ 0 & 0 & 0 \\ \mathcal{K}_{31} & 0 & 0 \end{pmatrix} + \begin{pmatrix} 0 & 0 & 0 \\ \mathcal{K}_{21} & 0 & 0 \\ 0 & \mathcal{K}_{32} & 0 \end{pmatrix} + \begin{pmatrix} \mathcal{K}_{11} & 0 & 0 \\ 0 & \mathcal{K}_{22} & \\ 0 & 0 & \mathcal{K}_{33} \end{pmatrix} + \begin{pmatrix} 0 & \mathcal{K}_{12} & 0 \\ 0 & 0 & \mathcal{K}_{23} \\ 0 & 0 & 0 \end{pmatrix} + \begin{pmatrix} 0 & 0 & \mathcal{K}_{13} \\ 0 & 0 & 0 \\ 0 & 0 & 0 \end{pmatrix}. \end{aligned} \quad (\text{A.12})$$

Then, the compactness of \mathcal{K} can be shown by induction. Indeed, since each term in this summation is compact for the same reasons outlined to prove the compactness of \mathcal{K}_d and \mathcal{K}_{od} in the 2×2 operator case, the $N \times N$ block operator \mathcal{K} is compact. \square

Appendix B. Analytic expression of the primal and dual Laplacian matrices

We provide here the analytic expression of the elements of the matrices $\mathbf{\Delta}_i$ and $\tilde{\mathbf{\Delta}}_i$ discretizing the Laplace-Beltrami operator by means of pyramid and dual pyramid functions as an implementation aid. In the following, we omit the subscript i that indicates the reference surface mesh $\Gamma_{h,i}$, its barycentric refinement $\tilde{\Gamma}_{h,i}$, or its dual counterpart $\tilde{\tilde{\Gamma}}_{h,i}$ and that is applied to matrices, basis functions, and geometrical entities of the mesh, to simplify the notation.

By analytic evaluation of $(\nabla_{\Gamma} \lambda_m, \nabla_{\Gamma} \lambda_n)_{L^2(\Gamma_h)}$, the expression

$$(\mathbf{\Delta})_{mn} = \begin{cases} \sum_{c \in \text{Adj}(v_m)} \frac{|e_{c,v_m}|^2}{4|c|} & \text{if } m = n \\ \sum_{c \in \text{Adj}(e_{mn})} \frac{|e_{c,v_m}| |e_{c,v_n}|}{4|c|} \cos(\theta_{c,mn}) & \text{if } v_m, v_n \text{ are connected by } e_{mn} \\ 0 & \text{otherwise} \end{cases} \quad (\text{B.1})$$

is retrieved, where $\text{Adj}(v_m)$ is the set of cells adjacent to the vertex v_m , $\text{Adj}(e_{mn})$ is the set of cells adjacent to the edge e_{mn} connecting vertex v_m and vertex v_n , $|e_{c,v_m}|$ is the length of the edge of cell c opposed to vertex v_m , $|c|$ denotes the area of cell c . As a general remark, the geometrical entities introduced up to now are elements of the primal mesh Γ_h , in symbols $v_m \in \Gamma_h$, $e_{c,v_m} \in \Gamma_h$, $e_{mn} \in \Gamma_h$, and $c \in \Gamma_h$. The angle $\theta_{c,mn}$ is defined as

$$\theta_{c,mn} := \theta_{c,m} + \theta_{c,n}, \quad (\text{B.2})$$

where $\theta_{c,m}$ is the interior angle of cell c at vertex v_m . In particular, given the length of the edges of c , it can be evaluated as

$$\theta_{c,m} = \text{angle} \left(|e_{mn}|, |e_{c,v_n}|, |e_{c,v_m}| \right), \tag{B.3}$$

where

$$\text{angle} (|e_1|, |e_2|, |e_3|) := \arccos \left(\frac{|e_1|^2 + |e_2|^2 - |e_3|^2}{2|e_1||e_2|} \right). \tag{B.4}$$

returns the interior angle of a triangle opposed to its edge e_3 with $|e_1|, |e_2|$, and $|e_3|$ denoting the length of the three sides of the triangle. The notation employed in equation (B.1) is shown in Figure B.9.

To define an analytic formula for the dual Laplacian matrix $\bar{\Delta}$, we express its elements as linear combinations of

$$(\bar{\Delta})_{mj,nk} = \left(\nabla_{\Gamma} \bar{\lambda}_{m,j}, \nabla_{\Gamma} \bar{\lambda}_{n,k} \right)_{L^2(\bar{\Gamma}_h)} \tag{B.5}$$

resulting in

$$(\bar{\Delta})_{mn} = \sum_{j=1}^7 \sum_{k=1}^7 \frac{1}{NoC(\bar{v}_{m,j})} \frac{1}{NoC(\bar{v}_{n,k})} (\bar{\Delta})_{mj,nk}, \tag{B.6}$$

where the notation applied is the same as in Section 2.4 (without the mesh index subscript i). The analytic expression of $(\bar{\Delta})_{mj,nk}$ is known from equation (B.1), as

$$(\bar{\Delta})_{mj,nk} = \begin{cases} \sum_{\bar{c} \in Adj(\bar{v}_{m,j})} \frac{|\bar{e}_{\bar{c},\bar{v}_{m,j}}|^2}{4|\bar{c}|} & \text{if } m = n \text{ and } j = k, \\ \sum_{\bar{c} \in Adj(\bar{e}_{mj,nk})} \frac{|\bar{e}_{\bar{c},\bar{v}_{m,j}}| |\bar{e}_{\bar{c},\bar{v}_{n,k}}|}{4|\bar{c}|} \cos(\theta_{\bar{c},mj,nk}) & \text{if } \bar{v}_{m,j}, \bar{v}_{n,k} \text{ are connected by } \bar{e}_{mj,nk}, \\ 0 & \text{otherwise.} \end{cases} \tag{B.7}$$

As above, the geometrical entities belonging to the barycentrically refined mesh $\bar{\Gamma}_h$ are denoted with an upper bar. In particular $Adj(\bar{v}_{m,j})$ is the set of cells of $\bar{\Gamma}_h$ adjacent to the vertex $\bar{v}_{m,j}$, $Adj(\bar{e}_{mj,nk})$ is the set of cells of $\bar{\Gamma}_h$ adjacent to the edge $\bar{e}_{mj,nk} \in \bar{\Gamma}_h$ connecting the vertices $\bar{v}_{m,j}$, and $\bar{v}_{n,k}$, $\bar{e}_{\bar{c},\bar{v}_{m,j}} \in \bar{\Gamma}_h$ is the edge of cell $\bar{c} \in \bar{\Gamma}_h$ opposed to $\bar{v}_{m,j} \in \bar{\Gamma}_h$, $|\bar{c}|$ is the area of cell $\bar{c} \in \bar{\Gamma}_h$. The angle $\theta_{\bar{c},mj,nk}$ is

$$\theta_{\bar{c},mj,nk} := \theta_{\bar{c},mj} + \theta_{\bar{c},nk}, \tag{B.8}$$

where $\theta_{\bar{c},mj}$ is the interior angle of the cell \bar{c} at the vertex $\bar{v}_{m,j}$.

All the quantities introduced in equation (B.7) are known from the geometrical properties of the primal mesh Γ_h . For example, by denoting as $c \subset \Gamma_h$ the cell containing $\bar{c} \subset \bar{\Gamma}_h$, we recognize that $|\bar{c}| = |c|/6$, directly following from the properties of the barycentric refinement. Moreover, the expression of the edge length $|\bar{e}_{\bar{c},\bar{v}_{m,j}}|$ reads

$$|\bar{e}_{\bar{c},\bar{v}_{m,j}}| = \begin{cases} \frac{1}{2}|e_{\bar{c}}| & \text{if } NoC(\bar{v}_{m,j}) = 1, \\ \frac{2}{3}|m_{\bar{c},\text{vert}}| & \text{if } NoC(\bar{v}_{m,j}) = 2, \\ \frac{1}{3}|m_{\bar{c},\text{side}}| & \text{otherwise,} \end{cases} \tag{B.9}$$

where $e_{\bar{c}}$ is the side of $c \supset \bar{c}$ with an infinite set of points in common with \bar{c} . We denote by $m_{\bar{c},\text{vert}}$ the median of $c \supset \bar{c}$ such that the intersection $m_{\bar{c},\text{vert}} \cap \bar{c}$ contains infinite points, including a vertex of c . The variable $m_{\bar{c},\text{side}}$ denotes the median of $c \supset \bar{c}$ such that the intersection $m_{\bar{c},\text{side}} \cap \bar{c}$ contains infinite points, but not including a vertex of c . Finally, the angle $\theta_{\bar{c},mj}$ can be retrieved as

$$\theta_{\bar{c},mj} = \begin{cases} \text{angle} \left(\frac{2}{3}|m_{\bar{c},\text{vert}}|, \frac{1}{3}|m_{\bar{c},\text{side}}|, \frac{1}{2}|e_{\bar{c}}| \right) & \text{if } NoC(\bar{v}_{m,j}) = 1, \\ \text{angle} \left(\frac{1}{3}|m_{\bar{c},\text{side}}|, \frac{1}{2}|e_{\bar{c}}|, \frac{2}{3}|m_{\bar{c},\text{vert}}| \right) & \text{if } NoC(\bar{v}_{m,j}) = 2, \\ \text{angle} \left(\frac{1}{2}|e_{\bar{c}}|, \frac{2}{3}|m_{\bar{c},\text{vert}}|, \frac{1}{3}|m_{\bar{c},\text{side}}| \right) & \text{otherwise.} \end{cases} \tag{B.10}$$

Figures B.10, B.11, and B.12 represent the notation employed.

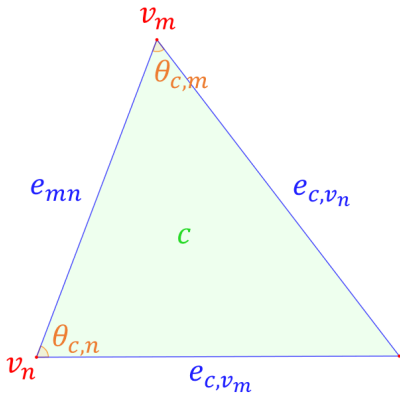


Fig. B.9. A primal cell in Γ_h with the notation for the definition of $(\Delta)_{mn}$ (equation (B.1)).

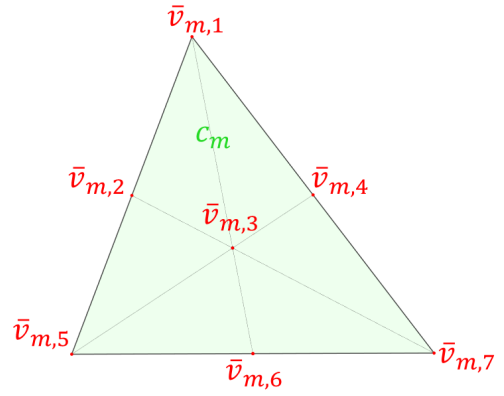


Fig. B.10. Seven vertices of $\bar{\Gamma}_i$ lie in the cell $c_m \in \Gamma_i$ (the numbering is randomly assigned).

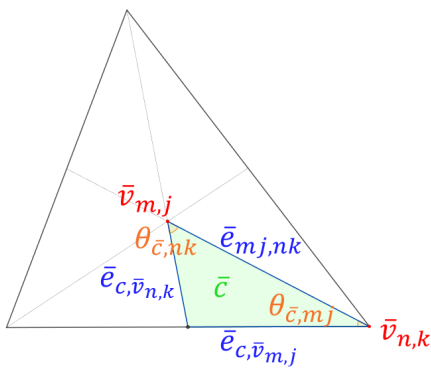


Fig. B.11. A cell in the barycentrically refined mesh $\bar{\Gamma}_h$ with the notation for the definition of $(\bar{\Delta})_{m_j,nk}$ (equation (B.7)).

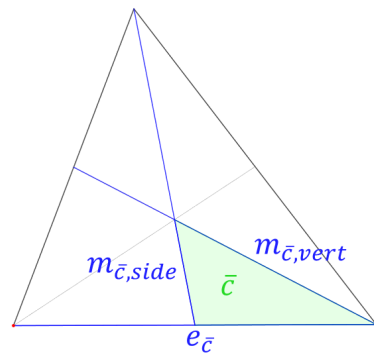


Fig. B.12. Notation for the definition of $|\bar{e}_{c,v_{m,j}}|$ (equation (B.9)) and θ_{c,m_j} (equation (B.10)).

Acknowledgment

This work was supported in part by the European Research Council (ERC) through the European Union's Horizon 2020 Research and Innovation Programme under Grant 724846 (Project 321), in part by the European Innovation Council (EIC) through the European Union's Horizon Europe research Programme under Grant 101046748 (Project CEREBRO), in part by the ANR Labex CominLabs under the project "CYCLE", and in part by the Italian Ministry of University and Research within the Program FARE, CELER, under Grant R187PMFXA4.

References

- [1] Y. Abramovich and C. Aliprantis. *An Invitation to Operator Theory*, volume 50 of *Graduate Studies in Mathematics*. American Mathematical Society, Providence, Rhode Island, September 2002. ISBN 978-0-8218-2146-6 978-1-4704-2099-4. doi: 10.1090/gsm/050.
- [2] S.B. Adrian, F.P. Andriulli, and T.F. Eibert. On a refinement-free Calderón multiplicative preconditioner for the electric field integral equation. *Journal of Computational Physics*, 376:1232–1252, January 2019. ISSN 00219991. doi: 10.1016/j.jcp.2018.10.009.
- [3] S.B. Adrian, A. Dely, D. Consoli, A. Merlini, and F.P. Andriulli. Electromagnetic integral equations: Insights in conditioning and preconditioning. *IEEE Open Journal of Antennas and Propagation*, 2:1143–1174, 2021. ISSN 2637-6431. doi: 10.1109/OJAP.2021.3121097.
- [4] Z. Akalin Acar and S. Makeig. Effects of forward model errors on EEG source localization. *Brain Topography*, 26(3):378–396, July 2013. ISSN 0896-0267, 1573-6792. doi: 10.1007/s10548-012-0274-6.
- [5] F.P. Andriulli, K. Cools, H. Bagci, F. Olyslager, A. Buffa, S. Christiansen, and E. Michielssen. A multiplicative Calderón preconditioner for the electric field integral equation. *IEEE Transactions on Antennas and Propagation*, 56(8):2398–2412, August 2008. ISSN 0018-926X. doi: 10.1109/TAP.2008.926788.
- [6] F.P. Andriulli, K. Cools, I. Bogaert, and E. Michielssen. On a well-conditioned electric field integral operator for multiply connected geometries. *IEEE Transactions on Antennas and Propagation*, 61(4):2077–2087, April 2013. ISSN 0018-926X, 1558-2221. doi: 10.1109/TAP.2012.2234072.
- [7] K.A. Awada, D.R. Jackson, J.T. Williams, D.R. Wilton, S.B. Baumann, and A.C. Papanicolaou. Computational aspects of finite element modeling in EEG source localization. *IEEE Transactions on Biomedical Engineering*, 44(8):736–752, Aug./1997. ISSN 00189294. doi: 10.1109/10.605431.
- [8] H. Bagci, F.P. Andriulli, K. Cools, F. Olyslager, and E. Michielssen. A Calderón multiplicative preconditioner for the combined field integral equation. *IEEE Transactions on Antennas and Propagation*, 57(10):3387–3392, October 2009. ISSN 0018-926X, 1558-2221. doi: 10.1109/TAP.2009.2029389.
- [9] S. Baillet, J.C. Mosher, and R.M. Leahy. Electromagnetic brain mapping. *Signal Processing Magazine, IEEE*, 18(6):14–30, 2001.
- [10] Y. Beghein, K. Cools, F.P. Andriulli, D. De Zutter, and E. Michielssen. A Calderón multiplicative preconditioner for the PMCHWT equation for scattering by chiral objects. *IEEE Transactions on Antennas and Propagation*, 60(9):4239–4248, September 2012. ISSN 0018-926X. doi: 10.1109/TAP.2012.2207061.
- [11] C.G. Bénar, D. Schön, S. Grimault, B. Nazarian, B. Burle, M. Roth, J.M. Badier, P. Marquis, C. Liegeois-Chauvel, and J.L. Anton. Single-trial analysis of oddball event-related potentials in simultaneous EEG-fMRI. *Human Brain Mapping*, 28(7):602–613, July 2007. ISSN 10659471, 10970193. doi: 10.1002/hbm.20289.
- [12] O Bertrand, F Perrin, and J Pernier. A theoretical justification of the average reference in topographic evoked potential studies. *Electroencephalography and Clinical Neurophysiology*, 62(6):3, 1985.
- [13] P. Bruno. A FDM anisotropic formulation for EEG simulation. *2006 International Conference of the IEEE Engineering in Medicine and Biology Society*, page 5, 2006.
- [14] M. Cheney, D. Isaacson, and J.C. Newell. Electrical impedance tomography. *Society for Industrial and Applied Mathematics*, 41(1):17, 1999.
- [15] M Clerc, G. Adde, J. Kybic, T. Papadopoulo, and J.M. Badier. In vivo conductivity estimation with symmetric boundary elements. *International Journal of Bioelectromagnetism*, 7(1):4, 2005.
- [16] D.L. Colton and R. Kress. *Integral Equation Methods in Scattering Theory*. Society for Industrial and Applied Mathematics, Philadelphia, 2013. ISBN 978-1-61197-315-0.
- [17] M. Costabel and E. Stephan. A direct boundary integral equation method for transmission problems. *Journal of Mathematical Analysis and Applications*, 106(2):367–413, March 1985. ISSN 0022247X. doi: 10.1016/0022-247X(85)90118-0.
- [18] M. Darbas. Generalized combined field integral equations for the iterative solution of the three-dimensional Maxwell equations. *Applied Mathematics Letters*, 19(8):834–839, August 2006. ISSN 08939659. doi: 10.1016/j.aml.2005.11.005.
- [19] M. Darbas and S. Lohrengel. Review on mathematical modelling of electroencephalography (EEG). *Jahresbericht der Deutschen Mathematiker-Vereinigung*, 121(1):3–39, March 2019. ISSN 0012-0456, 1869-7135. doi: 10.1365/s13291-018-0183-z.
- [20] J. C. de Munck. The potential distribution in a layered anisotropic spheroidal volume conductor. *Journal of Applied Physics*, 64(2):464–470, July 1988. ISSN 0021-8979, 1089-7550. doi: 10.1063/1.341983.
- [21] J.C. de Munck, B.W. van Dijk, and H. Spekreijse. Mathematical dipoles are adequate to describe realistic generators of human brain activity. *IEEE Transactions on Biomedical Engineering*, 35(11):960–966, Nov./1988. ISSN 00189294. doi: 10.1109/10.8677.
- [22] L.B. Felsen and N. Marcuvitz. *Radiation and Scattering of Waves*. John Wiley & Sons, January 1994. ISBN 978-0-7803-1088-9.
- [23] M. Fuchs, M. Wagner, and J. Kastner. Boundary element method volume conductor models for EEG source reconstruction. *Clinical Neurophysiology*, 112(8):1400–1407, August 2001. ISSN 13882457. doi: 10.1016/S1388-2457(01)00589-2.
- [24] V. Giunzioni, J.E. Ortiz G., A. Merlini, S.B. Adrian, and F.P. Andriulli. A new refinement-free preconditioner for the symmetric formulation in electroencephalography, April 2022.
- [25] S. Gonaves, J.C. de Munck, J.P.A. Verbunt, R.M. Heethaar, and F.H. Lopes da Silva. In vivo measurement of the brain and skull resistivities using an EIT-based method and the combined analysis of SEF/SEP data. *IEEE Transactions on Biomedical Engineering*, 50(9):1124–1128, September 2003. ISSN 0018-9294. doi: 10.1109/TBME.2003.816072.

- [26] R. Grech, T. Cassar, J. Muscat, K.P. Camilleri, S.G. Fabri, M. Zervakis, P. Xanthopoulos, V. Sakkalis, and B. Vanrumste. Review on solving the inverse problem in EEG source analysis. *Journal of NeuroEngineering and Rehabilitation*, 5(1):25, 2008. ISSN 1743-0003. doi: 10.1186/1743-0003-5-25.
- [27] H. Hallez, B. Vanrumste, R. Grech, J. Muscat, W. De Clercq, A. Vergult, Y. D'Asseler, K.P. Camilleri, S.G. Fabri, S. Van Huffel, and I. Lemahieu. Review on solving the forward problem in EEG source analysis. *Journal of NeuroEngineering and Rehabilitation*, 4(1):46, 2007. ISSN 1743-0003. doi: 10.1186/1743-0003-4-46.
- [28] B. He, T. Musha, Y. Okamoto, S. Homma, Y. Nakajima, and T. Sato. Electric dipole tracing in the brain by means of the boundary element method and its accuracy. *IEEE Transactions on Biomedical Engineering*, BME-34(6):406–414, June 1987. ISSN 0018-9294. doi: 10.1109/TBME.1987.326056.
- [29] C. Henry, A. Merlini, L. Rahmouni, and F.P. Andriulli. On a low-frequency and contrast stabilized full-wave volume integral equation solver for lossy media, August 2021.
- [30] M.R. Hestenes and E. Stiefel. Methods of conjugate gradients for solving linear systems. *Journal of Research of the National Bureau Standards*, 49(6):28, 1952.
- [31] G.C. Hsiao and R.E. Kleinman. Error analysis in numerical solution of acoustic integral equations. *International Journal for Numerical Methods in Engineering*, 37(17):2921–2933, September 1994. ISSN 0029-5981, 1097-0207. doi: 10.1002/nme.1620371705.
- [32] J. Jorge, F. Grouiller, R. Gruetter, W. van der Zwaag, and P. Figueiredo. Towards high-quality simultaneous EEG-fMRI at 7 T: Detection and reduction of EEG artifacts due to head motion. *NeuroImage*, 120:143–153, October 2015. ISSN 10538119. doi: 10.1016/j.neuroimage.2015.07.020.
- [33] L. Koessler, C. Benar, L. Maillard, J.M. Badier, J.P. Vignal, F. Bartolomei, P. Chauvel, and M. Gavaret. Source localization of ictal epileptic activity investigated by high resolution EEG and validated by SEEG. *NeuroImage*, 51(2):642–653, June 2010. ISSN 10538119. doi: 10.1016/j.neuroimage.2010.02.067.
- [34] P. Kolm, S. Jiang, and V. Rokhlin. Quadruple and octuple layer potentials in two dimensions I: Analytical apparatus. *Applied and Computational Harmonic Analysis*, 14(1):47–74, January 2003. ISSN 10635203. doi: 10.1016/S1063-5203(03)00004-6.
- [35] J. Kybic, M. Clerc, T. Abboud, O. Faugeras, R. Keriven, and T. Papadopoulo. A common formalism for the integral formulations of the forward EEG problem. *IEEE Transactions on Medical Imaging*, 24(1):12–28, January 2005. ISSN 0278-0062. doi: 10.1109/TMI.2004.837363.
- [36] X. Lei and K. Liao. Understanding the influences of EEG reference: A large-scale brain network perspective. *Frontiers in Neuroscience*, 11, April 2017. ISSN 1662-453X. doi: 10.3389/fnins.2017.00205.
- [37] C.M. Michel and D. Brunet. EEG source imaging: A practical review of the analysis steps. *Frontiers in Neurology*, 10:325, April 2019. ISSN 1664-2295. doi: 10.3389/fneur.2019.00325.
- [38] C.M. Michel and M.M. Murray. Towards the utilization of EEG as a brain imaging tool. *NeuroImage*, 61(2):371–385, June 2012. ISSN 10538119. doi: 10.1016/j.neuroimage.2011.12.039.
- [39] J.C. Nédélec. *Acoustic and Electromagnetic Equations*, volume 144 of *Applied Mathematical Sciences*. Springer New York, New York, NY, 2001. ISBN 978-1-4419-2889-4 978-1-4757-4393-7. doi: 10.1007/978-1-4757-4393-7.
- [40] Frank W. J. Olver and National Institute of Standards and Technology, editors. *NIST Handbook of Mathematical Functions*. Cambridge Univ. Press [u.a.], Cambridge, 2010. ISBN 978-0-521-19225-5 978-0-521-14063-8.
- [41] Michael O'Neil. Second-kind integral equations for the Laplace-Beltrami problem on surfaces in three dimensions. *Advances in Computational Mathematics*, 44(5):1385–1409, October 2018. ISSN 1019-7168, 1572-9044. doi: 10.1007/s10444-018-9587-7.
- [42] J.E. Ortiz G., A. Pillain, L. Rahmouni, and F.P. Andriulli. A Calderón regularized symmetric formulation for the electroencephalography forward problem. *Journal of Computational Physics*, 375:291–306, December 2018. ISSN 00219991. doi: 10.1016/j.jcp.2018.07.048.
- [43] R.D. Pascual-Marqui. Standardized low resolution brain electromagnetic tomography (sLORETA): Technical details. *Clinical Pharmacology, Methods & Findings in Experimental & Clinical Pharmacology*(24):16, 2002.
- [44] A. Pillain. *Line, Surface, and Volume Integral Equations for the Electromagnetic Modelling of the Electroencephalography Forward Problem*. PhD thesis, Ecole Nationale Supérieure des Télécommunications de Bretagne-ENSTB, 2017.
- [45] A. Pillain, L. Rahmouni, and F.P. Andriulli. Handling anisotropic conductivities in the EEG forward problem with a symmetric formulation. *Physics in Medicine & Biology*, 64(3):035022, February 2019. ISSN 1361-6560. doi: 10.1088/1361-6560/aafaf.
- [46] C. Plummer, A.S. Harvey, and Mark M. EEG source localization in focal epilepsy: Where are we now? *Epilepsia*, 49(2):201–218, February 2008. ISSN 0013-9580, 1528-1167. doi: 10.1111/j.1528-1167.2007.01381.x.
- [47] A. Quarteroni and A. Valli. *Numerical Approximation of Partial Differential Equations*, volume 23 of *Springer Series in Computational Mathematics*. Springer Berlin Heidelberg, Berlin, Heidelberg, 2008. ISBN 978-3-540-85267-4 978-3-540-85268-1. doi: 10.1007/978-3-540-85268-1.
- [48] L. Rahmouni, R. Mitharwal, and F.P. Andriulli. Two volume integral equations for the inhomogeneous and anisotropic forward problem in electroencephalography. *Journal of Computational Physics*, 348:732–743, November 2017. ISSN 00219991. doi: 10.1016/j.jcp.2017.07.013.
- [49] M.E. Raichle and M.A. Mintun. Brain work and brain imaging. *Annual Review of Neuroscience*, 29(1):449–476, July 2006. ISSN 0147-006X, 1545-4126. doi: 10.1146/annurev.neuro.29.051605.112819.
- [50] W. Rudin. *Principles of Mathematical Analysis*. International Series in Pure and Applied Mathematics. McGraw-Hill, New York, 3. ed., [nachdr.] edition, 2008. ISBN 978-0-07-054235-8.
- [51] J Sarvas. Basic mathematical and electromagnetic concepts of the biomagnetic inverse problem. *Physics in Medicine and Biology*, 32(1): 11–22, January 1987. ISSN 0031-9155, 1361-6560. doi: 10.1088/0031-9155/32/1/004.
- [52] S.A. Sauter and C. Schwab. *Boundary Element Methods*, volume 39 of *Springer Series in Computational Mathematics*. Springer Berlin Heidelberg, Berlin, Heidelberg, 2011. ISBN 978-3-540-68092-5 978-3-540-68093-2.
- [53] U. Schmitt, A.K. Louis, F. Darvas, H. Buchner, and M. Fuchs. Numerical aspects of spatio-temporal current density reconstruction from EEG-/MEG-data. *IEEE Transactions on Medical Imaging*, 20(4):314–324, April 2001. ISSN 02780062. doi: 10.1109/42.921480.
- [54] N.J. Shah, A.M. Oros-Peusquens, J. Arrubla, K. Zhang, T. Warbrick, K. Mauler, K. Vahedipour, S. Romanzetti, J. Felder, A. Celik, E. Rota-Kops, H. Iida, K.J. Langen, H. Herzog, and I. Neuner. Advances in multimodal neuroimaging: Hybrid MR–PET and MR–PET–EEG at 3 T and 9.4 T. *Journal of Magnetic Resonance*, 229:101–115, April 2013. ISSN 10907807. doi: 10.1016/j.jmr.2012.11.027.
- [55] J.R. Shewchuk. An introduction to the conjugate gradient method without the agonizing pain. page 64, 1994.
- [56] I.H. Sloan. Error analysis of boundary integral methods. *Acta Numerica*, 1:287–339, January 1992. ISSN 0962-4929, 1474-0508. doi:

- 10.1017/S0962492900002294.
- [57] P. Sonneveld. CGS, a fast Lanczos-type solver for nonsymmetric linear systems. *SIAM Journal on Scientific and Statistical Computing*, 10(1):36–52, January 1989. ISSN 0196-5204, 2168-3417. doi: 10.1137/0910004.
 - [58] T. Steihaug and M.R. Hestenes. Conjugate direction methods in optimization. *Mathematics of Computation*, 38(157):332, January 1982. ISSN 00255718. doi: 10.2307/2007488.
 - [59] O. Steinbach. *Numerical Approximation Methods for Elliptic Boundary Value Problems: Finite and Boundary Elements*. Springer, New York, 2008. ISBN 978-0-387-31312-2 978-0-387-68805-3.
 - [60] O. Steinbach and W. L. Wendland. The construction of some efficient preconditioners in the boundary element method. *Advances in Computational Mathematics*, 9(1-2):191–216, September 1998. ISSN 1019-7168, 1572-9044. doi: 10.1023/A:1018937506719.
 - [61] G. Strang. *Introduction to Linear Algebra*. Wellesley-Cambridge Press, Wellesley, Mass, 4. ed edition, 2009. ISBN 978-0-9802327-1-4 978-0-9802327-2-1.
 - [62] E. van't Wout, S.R. Haqshenas, P. G elat, T. Betcke, and N. Saffari. Benchmarking preconditioned boundary integral formulations for acoustics. *International Journal for Numerical Methods in Engineering*, 122(20):5873–5897, October 2021. ISSN 0029-5981, 1097-0207. doi: 10.1002/nme.6777.
 - [63] J. Vorwerk, M. Clerc, M. Burger, and C.H. Wolters. Comparison of boundary element and finite element approaches to the EEG forward problem. *Biomedical Engineering / Biomedizinische Technik*, 57(SI-1 Track-O), January 2012. ISSN 1862-278X, 0013-5585. doi: 10.1515/bmt-2012-4152.
 - [64] Y. Zhang, W. van Drongelen, and B. He. Estimation of *in vivo* brain-to-skull conductivity ratio in humans. *Applied Physics Letters*, 89(22):223903, November 2006. ISSN 0003-6951, 1077-3118. doi: 10.1063/1.2398883.
 - [65] Z. Zhang. A fast method to compute surface potentials generated by dipoles within multilayer anisotropic spheres. *Physics in medicine & biology*, 40(3):16, 1995.